Stochastic Topology Design Optimization for Continuous Elastic Materials.

Miguel Carrasco[1], Benjamin Ivorra[2], Angel Manuel Ramos[2]

[1] Facultad de Ingeniería y Ciencias Aplicadas,
Universidad de los Andes,
Av. San Carlos de Apoquindo 2200,
Santiago de Chile, Chile
email: migucarr@uandes.cl
[2] Departamento de Matemática Aplicada,
Universidad Complutense de Madrid &
Instituto de Matemática Interdisciplinar,
Plaza de Ciencias, 3, 28040–Madrid, Spain
email: ivorra@mat.ucm.es; angel@mat.ucm.es

July 8, 2014

Abstract

In this paper, we develop a stochastic model for topology optimization. We find robust structures that minimize the compliance for a given main load having a stochastic behavior. First, we give some properties about the stability of structures carrying several loads. Then, we propose a stochastic model that takes into account the expected value of the compliance and its variance. We show that, similarly to the case of truss structures, these values can be computed with an equivalent deterministic approach and the stochastic model can be transformed into a nonlinear programming problem, reducing the complexity of this kind of problems. Finally, we check our formulation by considering several 2D and 3D numerical examples. For each

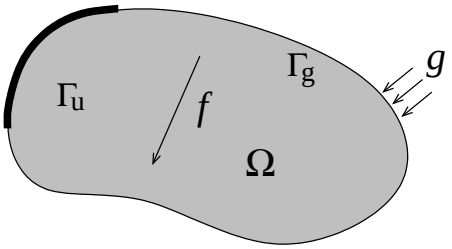

Figure 1: Representation of the elastic homogeneous body Ω and the considered external forces f and g.

benchmark case, we consider a set of optimization problems based on different weight coefficients of the compliance, expected-compliance and variance values and compare the robustness of the obtained solutions between them. We see that considering our methodology with an appropriate set of weight coefficients may help to generate structures robust to main loads and their perturbations.

Keywords: Topology optimization; Structural optimization; Stochastic programming; Finite element method.

1 Introduction

Let us consider an open set $\Omega \subset \mathbb{R}^d$, where d is 2 for planar structures or 3 for three-dimensional bodies. The set Ω represents a body that we assume is made of an isotropic, homogeneous and linear elastic material. The boundary of Ω is denoted here by $\partial\Omega = \Gamma_u \cup \Gamma_g$ with $\Gamma_u \cap \Gamma_g = \emptyset$. In this setting, Γ_u corresponds to the part of the boundary of Ω where the displacements of the body are not allowed. We assume that external forces f and g are applied to Ω and Γ_g, respectively. A graphical representation of Ω is given in Figure 1.

The displacements can be computed (see e.g. [1]) by solving the following system of partial differential equations:

$$\begin{cases} -\operatorname{div}(K\, e(u)) &= f, \quad \text{in } \Omega, \\ u &= 0, \quad \text{on } \Gamma_u, \\ (K\, e(u)) \cdot \hat{n} &= g, \quad \text{on } \Gamma_g, \end{cases} \tag{1}$$

where $u \colon \Omega \to \mathbb{R}^d$ is the vector of displacements, $e(u) = \frac{1}{2}(\nabla u + \nabla u^t)$ denotes

the linearized strain tensor, K is the fourth-order material elasticity tensor, $\mathrm{div}(\cdot)$ is the divergence of a tensor field and $\hat{n}$ is the outward unit normal vector on the boundary of the domain. We suppose that $K \in M$, which is a set of admissible stiffness tensors, related to the admissible materials we might use. Typically (see [2, 3]), the set of admissible tensor M is a subset of

$$\hat{M} = \left\{ \eta(x) K^0 \;\middle|\; 0 \leq \int_\Omega \eta(x)\,\mathrm{d}x \leq V_{\max} \text{ and } \eta\colon \Omega \to [\eta_{\min}, \eta_{\max}] \right\}, \qquad (2)$$

where $V_{\max}$ is the maximum amount of material that is allocated; $\eta(x)$ is the density of material at point $x \in \Omega$; $\eta_{\min} > 0$, $\eta_{\max}$ the maximum density we may use; and K^0 the fourth-order tensor of the considered linear elastic isotropic material. Additionally, other constrains should be considered in order to obtain physically realizable structures. For example, we would like to avoid structures with intermediate density zones (i.e., $\eta(x) \in]\eta_{\min}, \eta_{\max}[$), and microstructures with periodic variation density. For practical reasons, these constraints are not detailed in the continuous definition of M but they will be taken into account in its numerical implementation (see Section 4).

In the following, we assume that $f \in L^2(\Omega)^d$ and $g \in L^2(\Gamma_g)^d$ although less regular external forces can be also considered (see Remark 1 below)

Let us define $H = \{u \in [H^1(\Omega)]^d \mid u|_{\Gamma_u} = 0\}$, where the space $H^1(\Omega)$ is the well-known Sobolev space of functions that are in $L^2(\Omega)$ with the first derivatives (in the sense of distributions) in $L^2(\Omega)$. For a given material and its corresponding stiffness tensor $K \in M$, following [2, 4] we define the bilinear functional $A_K\colon H \times H \to \mathbb{R}$ by

$$A_K(u, v) := \int_\Omega e(u) : Ke(v)\,\mathrm{d}x, \qquad (3)$$

where $e(u) : Ke(v)$ denotes the tensor product given by

$$e(u) : Ke(v) := \sum_{i,j,k,l=1}^{d} K_{ijkl} e_{ij}(u) e_{ij}(v).$$

We recall that a weak solution of system (1) is a vector $u \in H$ satisfying

$$A_K(u, v) = \int_\Omega f \cdot v\,\mathrm{d}x + \int_{\Gamma_g} g \cdot v\,\mathrm{d}x \qquad \forall v \in H. \qquad (4)$$

We note that, under suitable conditions on the data (according to Korn's inequality and the Lax-Milgram Lemma [5, 6]), Problem (1) has a unique weak solution (see [7] for more details).

Remark 1 *In this work it is possible to include functions less regular than $f \in L^2(\Omega)$ or $g \in L^2(\Gamma_g)$ with a suitable alternative weak formulation instead of (4). An example of force $f \notin L^2(\Omega)$ that is typically considered is a point wise force $f = \delta(x-a)$, where $\bar{f} \in \mathbb{R}^d$ and $a \in \bar{\Omega}$. In this case, $\int_\Omega f \cdot v \, \mathrm{d}x = \bar{f} v(a)$. Nevertheless, when computing an approximated solution by using the Finite Element Method (see Section 4) f and g are usually approximated by functions in $L^2(\Omega)^d$ and $L^2(\Gamma_g)^d$, respectively, and (4) can be used again, becoming a linear system in finite dimension.*

For the sake of simplicity and without loss of generality, in the following, we only develop the case when $g = 0$. To recover the general case, the reader should replace $\int_\Omega f \cdot v \, \mathrm{d}x$ by $\int_\Omega f \cdot v \, \mathrm{d}x + \int_{\Gamma_g} g \cdot v \, \mathrm{d}x$, keeping in mind that the integral notation should be changed by suitable duality products for cases with less regular forces.

We note that, due to the symmetry of operator $A_K(\cdot,\cdot)$, equation (4) (with $g = 0$) above can be seen as the optimality condition of the following problem

$$\frac{1}{2}\int_\Omega f \cdot u \, \mathrm{d}x = \max_{v \in H} \left\{ \int_\Omega f \cdot v \, \mathrm{d}x - \frac{1}{2} A_K(v,v) \right\}. \tag{5}$$

The optimal value of the problem above is called *compliance* (see e.g. [2]) and can be seen as a measure of the global stiffness of a given material. Under this setting the well known minimum compliance topology design problem corresponds to (see [3, 2])

$$\min_{K \in M} \left\{ \frac{1}{2}\int_\Omega f \cdot u \, \mathrm{d}x, \quad \text{where } u \in H \text{ satisfies:} \right. \\ \left. A_K(u,v) = \int_\Omega f \cdot v \, \mathrm{d}x \ \ \forall v \in H \right\}. \tag{6}$$

Our main purpose is to find an optimal material in the set M (minimum compliance) when the external load force has a stochastic behavior. In an analogous way to previous stochastic results for truss optimization (see [8, 9, 10] and the next section), we assume that the external load force

f is perturbed by a $L^2(\Omega)^d$-valued random variable $\xi\colon \mathcal{B} \to L^2(\Omega)^d$, where $(\mathcal{B}, \mathcal{F}, \mathbb{P})$ is a probability space[1], with expected value

$$\mathbb{E}(\xi) = \int_{\mathcal{B}} \xi \, \mathrm{d}\mathbb{P} = \int_{\mathcal{B}} \xi(\omega) \, \mathbb{P}(\mathrm{d}\omega) = 0 \in L^2(\Omega)^d.$$

Remark 2 *Similarly, when $g \neq 0$, the surface load is perturbed by a $L^2(\Gamma_g)^d$ – valued random variable $\xi\colon \mathcal{B} \to L^2(\Gamma_g)^d$ with $\mathbb{E}(\xi) = 0$.*

For a given material $K \in M$ and a random perturbation ξ, we have the corresponding compliance

$$\begin{aligned} \Psi(\xi, K) = \int_\Omega (f + \xi) \cdot u \, \mathrm{d}x, \quad & \text{where } u \in H \text{ satisfies:} \\ A_K(u, v) = \int_\Omega (f + \xi) \cdot v \, \mathrm{d}x \quad & \text{for all } v \text{ in } H. \end{aligned} \tag{7}$$

Following [8, 2, 4], we state the stochastic topology design problem as

$$\min_{K \in M} \mathbb{E}[\Psi(\xi, K)], \tag{8}$$

where the expected value of the random variable $\Psi(\xi, K)$ is given by

$$\mathbb{E}(\Psi(\xi, K)) = \int_{\mathcal{B}} \Psi(\xi(\omega), K) \, \mathbb{P}(\mathrm{d}\omega).$$

We note that, when the support of the probability distribution is the singleton $\{0\}$, i.e. $\mathcal{B} = \{\xi = 0\}$ and $\mathbb{P}\{\xi = 0\} = 1$, Problem (8) corresponds to the minimum compliance design model (6). Also when the probability distribution has finite support we obtain the well known *multiload model* (see [2, 3]). We recall that the multiload model was proposed in order to take into account several loading scenarios or loads that are applied in different instant of time. This model corresponds to the minimization of a weighted average of the compliance. More precisely, if we consider the functions $f_i\colon \Omega \to \mathbb{R}^d$, for $i = 1, \ldots, k$, and the functional $A_K(\cdot, \cdot)$ defined in eq. (4), the multiload model is given by

$$\min_{K \in M} \left\{ \sum_i w_i \int_\Omega f_i \cdot u_i \, \mathrm{d}x, \quad \text{where } u_i \in H \text{ satisfies:} \right. \\ \left. A_K(u_i, v) = \int_\Omega f_i \cdot v \, \mathrm{d}x, \quad \text{for all } v \text{ in } H \right\}. \tag{9}$$

[1]With this notation $\mathcal{B}$ is the sample space, $\mathcal{F}$ denotes the σ-field and $\mathbb{P}$ its probability measure.

Taking the discrete probability law given by $\mathcal{B} = \{\xi = f_1, \ldots, \xi = f_k\}$ and $f = 0$, defining the weights as $w_i := \mathbb{P}\{\xi = f_i\}$ (the probability that discrete variable ξ take the value f_i), we get that the previous problem is a particular case of (8), and therefore, the proposed model extends classical formulations.

In [11] formulation (8) was studied for some choices of the random variable ξ and good results were obtained. From a theoretical point of view, it is showed that the expected value can be computed with an equivalent deterministic approach which reduces drastically the computational cost of computing a solution of the stochastic Problem (8) (see Section 3 for a summary of these results). Numerical experiments have been carried out for some particular benchmarks using the expected compliance formulation (8). Recently, a new approach based on numerical and Monte Carlo methods has been proposed by Zhao and Wan (see [12]) in order to obtain robust structures under load uncertainty. In other direction, Allaire (see [13]) proposes a deterministic method for optimizing a structure with respect to its worst possible behavior. Similarly to the case of trusses (see [10]) this approach provides solutions which are robust under load perturbations, but for some particular scenarios it may happen that the value of the compliance is too large and this model is no suitable. In order to avoid this situation we propose the following alternative.

$$\min_{K \in M} \{\alpha \mathbb{E}[\Psi(\xi, K)] + \beta \operatorname{Var}[\Psi(\xi, K)]\}, \tag{10}$$

where $\alpha, \beta \in [0, 1]$ and Var is the variance of the random variable $\Psi(\xi, K)$.

In Section 5, we illustrate the interest of formulation (10) by considering various 2D and 3D benchmark problems. We consider a set of values for (α, β), and compare the different solutions in terms of robustness to the main load and its perturbations.

2 About the stability of bodies submitted to several loads

There are several examples with trusses (see e.g. [8, 14]) showing that optimized structures obtained by the classical model (6) could produce unstable mechanical behaviors. Numerically, we have that the corresponding stiffness matrix associated to the finite element discretization is close to be singular and therefore it may produce an extremely large value of the compliance.

The multiload model described in the previous section, see Eq. (9), helps to avoid this problem by considering several loading scenarios. The following theorem about the stability of structures helps to understand the behavior of a structure submitted to several loading scenarios. Similar result for trusses can be found in Alvarez and Carrasco [8].

Let $K \in M$ a tensor representing a given material and $f_i \colon \Omega \to \mathbb{R}^d,\ i = 1, \dots, k$. We denote by

$$\mathrm{Conv}\{f_i\}_1^k := \left\{ \sum_{i=1}^k \lambda_i f_i \;\middle|\; \sum_{i=1}^k \lambda_i \leq 1, \lambda_i \geq 0,\ i = 1, \dots, k \right\},$$

the convex hull of functions $f_i, i = 1, \dots, k$.

Theorem 1 *Let us consider $f \in \mathrm{Conv}\{f_i\}_1^k$ and we consider $u_i \in H,\ i = 1, \dots, k$, such that*

$$A_K(u_i, v) = \int_\Omega f_i \cdot v \, \mathrm{d}x \quad \textit{for all } v \in H. \tag{11}$$

Then, if $u \in H$ is the solution of (4) it satisfies

$$\int_\Omega f \cdot u \, \mathrm{d}x \leq \max_{1 \leq i \leq k} \left\{ \int_\Omega f_i \cdot u_i \, \mathrm{d}x \right\}. \tag{12}$$

Proof: Let $\{\lambda\}_{i=1}^k \subset [0, 1]$, with $\sum_{i=1}^k \lambda_i \leq 1$. We define $f \colon \Omega \to \mathbb{R}^d$ as the function $x \mapsto f(x) = \sum_{i=1}^k \lambda_i f_i(x)$. Using that $A_K(\cdot, \cdot)$ is coercive and by the definition of f, it follows, for all $v \in H$

$$\begin{aligned} \int_\Omega f \cdot v \, \mathrm{d}x - \tfrac{1}{2} A_K(v, v) &= \int_\Omega f \cdot v \, \mathrm{d}x - \tfrac{1}{2} \sum_{i=1}^k \lambda_i A_K(v, v) \\ &= \sum_{i=1}^k \lambda_i \left\{ \int_\Omega f_i \cdot v \, \mathrm{d}x - \tfrac{1}{2} A_K(v, v) \right\}. \end{aligned}$$

Now from the optimality condition Eq. (5) (with f_i instead of f) and using equation (11), we obtain

$$\int_\Omega f \cdot v \, \mathrm{d}x - \tfrac{1}{2} A_K(v, v) \leq \tfrac{1}{2} \sum_{i=1}^k \lambda_i \int_\Omega f_i \cdot u_i \, \mathrm{d}x \quad \text{for all } v \in H,$$

and therefore,

$$\int_\Omega f \cdot v \, \mathrm{d}x - \tfrac{1}{2} A_K(v,v) \leq \tfrac{1}{2} \max_{1 \leq i \leq k} \int_\Omega f_i \cdot u_i \, \mathrm{d}x \quad \text{for all } v \in H.$$

Consequently,

$$\sup_{v \in H} \left\{ \int_\Omega f \cdot v \, \mathrm{d}x - \tfrac{1}{2} A_K(v,v) \right\} \leq \tfrac{1}{2} \max_{1 \leq i \leq k} \int_\Omega f_i \cdot u_i \, \mathrm{d}x.$$

We note that, by the bilinearity of $A_K(\cdot,\cdot)$, we have that function $u = \sum_{i=1}^k \lambda_i u_i$ is the unique solution of (4), since

$$A_K(u,v) = \sum_{i=1}^k \lambda_i A_K(u_i,v) = \sum_{i=1}^k \lambda_i \int_\Omega f_i \cdot v \, \mathrm{d}x \quad \text{for all } v \in H.$$

Therefore, using the optimality condition (5) we conclude

$$\int_\Omega f \cdot u \, \mathrm{d}x = 2 \max_{v \in H} \left\{ \int_\Omega f \cdot v \, \mathrm{d}x - \tfrac{1}{2} A_K(v,v) \right\} \leq \max_{1 \leq i \leq k} \int_\Omega f_i \cdot u_i \, \mathrm{d}x.$$

□

Theorem 1 implies that the compliance of any load in $\mathrm{Conv}\{f_i\}_1^k$ is bounded by the maximum value of the compliances of each f_i. It is easy to see, that (12) is also true for $f \in \mathrm{Conv}\{f_i, -f_i\}_1^k$.

3 Variance-expected compliance approach for topology optimization

3.1 Variance-expected approach

In this section, we study the stochastic topology design problem (10) proposed in Section (1). We show that this problem can be transformed into a multiload like problem in which the loading scenarios are related to the variance of random loads applied to Ω.

Firstly, we consider the stochastic topology optimization problem (8). In the following, we will consider the set $\{P_i\}_{i=1}^\infty \subset L^2(\Omega)^d$, corresponding to directions of perturbation of the main force $f \in L^2(\Omega)$. As said in Remark 1, spaces less regular that $L^2(\Omega)^d$ can be also considered.

Theorem 2 below gives an explicit expression of Problem (8) which can be directly evaluated. Therefore, a *Monte-Carlo* algorithm (see [15]), which is usually numerically expensive, is not necessary to approximate the value of $\mathbb{E}[\Psi(\xi, K)]$. The proof of this theorem can be found in [11].

Theorem 2 *With the notation introduced above let us consider* $\xi\colon \mathcal{B} \to L^2(\Omega)^d$ *be a random load, which in terms of the directions* $\{P_i\}_{i=1}^{\infty}$ *is written as* $\xi(\omega) = \sum_{i=1}^{\infty} \varepsilon_i(\omega) P_i$, *where* $\{\varepsilon_i\}_{i=1}^{\infty}$ *are independent random variables such that* $\mathbb{E}(\varepsilon_i) = 0$, $\mathbb{E}(\varepsilon_i \varepsilon_j) = 0$ *for* $i \neq j$, *and* $\mathrm{Var}(\varepsilon_i) = \sigma_i^2$. *Then the stochastic problem defined in* (8) *can be rewritten as the multiload problem:*

$$\min_{K \in M} \int_\Omega f \cdot u \, \mathrm{d}x + \sum_{i=1}^{+\infty} \int_\Omega \sigma_i P_i \cdot U_i \, \mathrm{d}x, \tag{13}$$

$$u \in H \text{ such that } A_K(u, v) = \int_\Omega f \cdot v \, \mathrm{d}x, \ \forall v \in H, \tag{14}$$

$$U_i \in H \text{ such that } A_K(U_i, v) = \int_\Omega \sigma_i P_i \cdot v \, \mathrm{d}x, \ \forall v \in H, \ \forall\, i \in \mathbb{N}. \tag{15}$$

Remark 3 *Normal distribution* $\varepsilon_i \sim \mathcal{N}(0, \sigma_i^2)$ *satisfy the assumptions in Theorem* (2) *(see* (23)*).*

Remark 4 *It can be proved that* $L^2(\Omega)^d$ *(also* $L^2(\Gamma_g)^d$ *and many other spaces suitable for cases with* f *and* g *less regular) is a separable Hilbert space and, therefore, there exist a Hilbert basis* $\{P_i\}_{i=1}^{\infty} \subset L^2(\Omega)^d$. *So that, for any* $\xi \in L^2(\Omega)^d$ *there exists* $\{\varepsilon_i\}_{i=1}^{\infty} \subset \mathbb{R}$ *such that* $\xi = \sum_{i=1}^{\infty} \varepsilon_i P_i$.

In order to avoid scenarios with too large values of the compliance we can consider Problem (10).

Let us define the inverse functional $G\colon [L^2(\Omega)]^d \to H$ by $G(f) = u$, where u is the (unique) weak solution of (1) or, equivalently, (4) or (5).

Then, for a given random perturbation $\xi \in L^2(\Omega)^d$ and a tensor $K \in M$ we have that

$$\Psi(\xi, K) = \int_\Omega (f + \xi) \cdot G(f + \xi) \, \mathrm{d}x.$$

The variance of $\Psi(\xi, K)$ is computed by using the well known formula

$$\mathrm{Var}[\Psi(\xi, K)] = \mathbb{E}[\Psi(\xi, K)^2] - \mathbb{E}[\Psi(\xi, K)]^2. \tag{16}$$

Let us consider $\xi = \sum_{i=1}^{m} \varepsilon_i P_i$, where $P_i \in [L^2(\Omega)]^d$ for $i = 1, \ldots, m$, and ε_i are real random variables that satisfy $\mathbb{E}(\varepsilon_i) = 0$ for $i = 1, \ldots, m$. Using the linearity of operator $G(\cdot)$, defined above, we can calculate explicitly the value of $\mathrm{Var}[\Psi(\xi, K)]$, by using the following identities

$$\mathbb{E}\left[\left(\int_\Omega f \cdot G(\xi)\,\mathrm{d}x\right)^2\right] = \sum_{i,j=1}^{m} \mathbb{E}(\varepsilon_i\varepsilon_j) \int_\Omega f \cdot G(P_i)\,\mathrm{d}x \int_\Omega f \cdot G(P_j)\,\mathrm{d}x, \quad (17)$$

$$\mathbb{E}\left[\left(\int_\Omega \xi \cdot G(f)\,\mathrm{d}x\right)^2\right] = \sum_{i,j=1}^{m} \mathbb{E}(\varepsilon_i\varepsilon_j) \int_\Omega P_i \cdot G(f)\,\mathrm{d}x \int_\Omega P_j \cdot G(f)\,\mathrm{d}x, \quad (18)$$

$$\mathbb{E}\left[\int_\Omega f \cdot G(\xi)\,\mathrm{d}x \int_\Omega \xi \cdot G(f)\,\mathrm{d}x\right] = \sum_{i,j=1}^{m} \mathbb{E}(\varepsilon_i\varepsilon_j) \int_\Omega f \cdot G(P_i)\,\mathrm{d}x \int_\Omega P_j \cdot G(f)\,\mathrm{d}x, \quad (19)$$

$$\mathbb{E}\left[\int_\Omega f \cdot G(\xi)\,\mathrm{d}x \int_\Omega \xi \cdot G(\xi)\,\mathrm{d}x\right] = \sum_{i,j,k=1}^{m} \mathbb{E}(\varepsilon_i\varepsilon_j\varepsilon_k) \int_\Omega f \cdot G(P_i)\,\mathrm{d}x \int_\Omega P_j \cdot G(P_k)\,\mathrm{d}x, \quad (20)$$

$$\mathbb{E}\left[\int_\Omega \xi \cdot G(f)\,\mathrm{d}x \int_\Omega \xi \cdot G(\xi)\,\mathrm{d}x\right] = \sum_{i,j,k=1}^{m} \mathbb{E}(\varepsilon_i\varepsilon_j\varepsilon_k) \int_\Omega P_i \cdot G(f)\,\mathrm{d}x \int_\Omega P_j \cdot G(P_k)\,\mathrm{d}x, \quad (21)$$

$$\mathbb{E}\left[\left(\int_\Omega \xi \cdot G(\xi)\,\mathrm{d}x\right)^2\right] = \sum_{i,j,k,l=1}^{m} \mathbb{E}(\varepsilon_i\varepsilon_j\varepsilon_k\varepsilon_l) \int_\Omega P_i \cdot G(P_j)\,\mathrm{d}x \int_\Omega P_k \cdot G(P_l)\,\mathrm{d}x. \quad (22)$$

In the particular case in which ε_i are independent random variables, with $\varepsilon_i \sim \mathcal{N}(0, \sigma_i^2)$ for $i = 1, \ldots, m$, we get

$$\mathbb{E}(\varepsilon_i \varepsilon_j) = \begin{cases} \sigma_i^2 & \text{if } i = j \\ 0 & \text{if } i \neq j \end{cases}, \quad \mathbb{E}(\varepsilon_i \varepsilon_j \varepsilon_k) = 0,$$

$$\mathbb{E}(\varepsilon_i \varepsilon_j \varepsilon_k \varepsilon_l) = \begin{cases} 3\sigma_i^4 & \text{if } i = j = k = l, \\ \sigma_i^2 \sigma_j^2 & \text{if } i = k, j = l \text{ or } i = l, j = k \text{ and } i \neq j, \\ \sigma_i^2 \sigma_k^2 & \text{if } i = j, k = l \text{ and } i \neq k, \\ 0 & \text{either case.} \end{cases} \tag{23}$$

The following theorem shows the particular case of two perturbation functions, and corresponds to the formulation used in the numerical test given in the next section

Theorem 3 *Using the notation of the previous theorem, let us consider a random perturbation of f given by $\xi = \varepsilon_1 P_1 + \varepsilon_2 P_2$, where the perturbation functions $P_1, P_2 \in L^2(\Omega)^d$ and $\varepsilon_1, \varepsilon_2$ are independent random variables, with $\varepsilon_i \sim \mathcal{N}(0, \sigma_i^2)$. Then*

$$\begin{aligned} \mathrm{Var}[\Psi(\xi, K)] = &\left(\int_\Omega f \cdot U_1 \, \mathrm{d}x + \int_\Omega \sigma_1 P_1 \cdot u \, \mathrm{d}x \right)^2 \\ &+ \left(\int_\Omega f \cdot U_2 \, \mathrm{d}x + \int_\Omega \sigma_2 P_2 \cdot u \, \mathrm{d}x \right)^2 \\ &+ \left(\int_\Omega \sigma_1 P_1 \cdot U_2 \, \mathrm{d}x + \int_\Omega \sigma_2 P_2 \cdot U_1 \, \mathrm{d}x \right)^2 + \\ &2 \left(\int_\Omega \sigma_1 P_1 \cdot U_1 \, \mathrm{d}x \right)^2 + 2 \left(\int_\Omega \sigma_2 P_2 \cdot U_2 \, \mathrm{d}x \right)^2, \end{aligned}$$

where $u = G(f), U_i = G(\sigma_i P_i)$, $i = 1, 2$. In other words,

$$A_K(u, v) = \int_\Omega f \cdot v \, \mathrm{d}x, \; A_K(U_i, v) = \int_\Omega \sigma_i P_i \cdot v \, \mathrm{d}x, \; \forall v \in H, \; i = 1, 2.$$

Proof: First, we recall that for a given random variable X and a constant $a \in \mathbb{R}$ we have the following properties we use

$$\mathrm{Var}(a + X) = \mathrm{Var}(X) = \mathbb{E}(X^2) - \mathbb{E}(X)^2, \tag{24}$$

Additionally, as $\mathbb{E}(\xi) = 0$ and using the linearity of operator $G(\cdot)$, we obtain

$$\mathbb{E}\left[\int_\Omega f \cdot G(\xi) + \xi \cdot G(f) + \xi \cdot G(\xi)\,\mathrm{d}x\right] = \mathbb{E}\left[\int_\Omega \xi \cdot G(\xi)\,\mathrm{d}x\right]. \tag{25}$$

Therefore, using (24)-(25) we get

$$\begin{aligned}
\mathrm{Var}[\Psi(\xi, K)] &= \mathrm{Var}\left[\int_\Omega (f+\xi)\cdot(G(f+\xi))\,\mathrm{d}x\right] \\
&= \mathrm{Var}\left[\int_\Omega f \cdot G(\xi) + \xi \cdot G(f) + \xi \cdot G(\xi)\,\mathrm{d}x\right] \\
&= \mathbb{E}\left[\left(\int_\Omega f \cdot G(\xi) + \xi \cdot G(f) + \xi \cdot G(\xi)\,\mathrm{d}x\right)^2\right] \\
&\quad - \left(\mathbb{E}\left[\int_\Omega \xi \cdot G(\xi)\,\mathrm{d}x\right]\right)^2.
\end{aligned}$$

Using (17)-(21) combined with (23) we obtain the following relations

$$\mathbb{E}\left[\left(\int_\Omega f \cdot G(\xi)\,\mathrm{d}x\right)^2\right] = \sigma_1^2\left(\int_\Omega f \cdot G(P_1)\,\mathrm{d}x\right)^2 + \sigma_2^2\left(\int_\Omega f \cdot G(P_2)\,\mathrm{d}x\right)^2,$$

$$\mathbb{E}\left[\left(\int_\Omega \xi \cdot G(f)\,\mathrm{d}x\right)^2\right] = \sigma_1^2\left(\int_\Omega P_1 \cdot G(f)\,\mathrm{d}x\right)^2 + \sigma_2^2\left(\int_\Omega P_2 \cdot G(f)\,\mathrm{d}x\right)^2,$$

$$\begin{aligned}
&\mathbb{E}\left[\int_\Omega f \cdot G(\xi)\,\mathrm{d}x \int_\Omega \xi \cdot G(f)\,\mathrm{d}x\right] = \\
&\quad \sigma_1^2 \int_\Omega f \cdot G(P_1)\,\mathrm{d}x \int_\Omega P_1 \cdot G(f)\,\mathrm{d}x + \sigma_2^2 \int_\Omega f \cdot G(P_2)\,\mathrm{d}x \int_\Omega P_2 \cdot G(f)\,\mathrm{d}x,
\end{aligned}$$

$$\mathbb{E}\left[\int_\Omega f \cdot G(\xi)\,\mathrm{d}x \int_\Omega \xi \cdot G(\xi)\,\mathrm{d}x\right] = \mathbb{E}\left[\int_\Omega \xi \cdot G(f)\,\mathrm{d}x \int_\Omega \xi \cdot G(\xi)\,\mathrm{d}x\right] = 0.$$

Therefore,

$$\begin{aligned}
\mathrm{Var}[\Psi(\xi, K)] &= \sigma_1^2\left(\int_\Omega f \cdot G(P_1)\,\mathrm{d}x + \int_\Omega P_1 \cdot G(f)\,\mathrm{d}x\right)^2 \\
&\quad + \sigma_2^2\left(\int_\Omega f \cdot G(P_2)\,\mathrm{d}x + \int_\Omega P_2 \cdot G(f)\,\mathrm{d}x\right)^2 \\
&\quad + \mathbb{E}\left[\left(\int_\Omega \xi \cdot G(\xi)\,\mathrm{d}x\right)^2\right] - \left(\mathbb{E}\left[\int_\Omega \xi \cdot G(\xi)\,\mathrm{d}x\right]\right)^2.
\end{aligned} \tag{26}$$

On the other hand, from (22) and (23) we have

$$\begin{aligned}\mathbb{E}\left[\left(\int_\Omega \xi\cdot G(\xi)\,\mathrm{d}x\right)^2\right] &= 3\sigma_1^4\left(\int_\Omega P_1\cdot G(P_1)\,\mathrm{d}x\right)^2 + 3\sigma_2^4\left(\int_\Omega P_2\cdot G(P_2)\,\mathrm{d}x\right)^2\\ &\quad+\sigma_1^2\sigma_2^2\left(\int_\Omega P_1\cdot G(P_2)\,\mathrm{d}x\right)^2+\sigma_1^2\left(\int_\Omega P_2\cdot G(P_1)\,\mathrm{d}x\right)^2\\ &\quad+2\sigma_1^2\sigma_2^2\left(\int_\Omega P_1\cdot G(P_1)\,\mathrm{d}x\int_\Omega P_2\cdot G(P_2)\,\mathrm{d}x\right.\\ &\qquad\left.+\int_\Omega P_1\cdot G(P_2)\,\mathrm{d}x\int_\Omega P_2\cdot G(P_1)\,\mathrm{d}x\right)\end{aligned}$$

Additionally, using that $\mathbb{E}(\varepsilon_1\varepsilon_2)=0$ we obtain

$$\begin{aligned}\mathbb{E}\left[\int_\Omega \xi\cdot G(\xi)\,\mathrm{d}x\right] &= \mathbb{E}\left[\int_\Omega \varepsilon_1^2 P_1\cdot G(P_1)+\varepsilon_2^2 P_2\cdot G(P_2)+\varepsilon_1\varepsilon_2 P_2\cdot G(P_1)\right.\\ &\qquad\left.+\varepsilon_1\varepsilon_2 P_1\cdot G(P_2)\,\mathrm{d}x\right]\\ &= \sigma_1^2\int_\Omega P_1\cdot G(P_1)\,\mathrm{d}x+\sigma_2^2\int_\Omega P_2\cdot G(P_2)\,\mathrm{d}x.\end{aligned}$$

Thus,

$$\begin{aligned}&\mathbb{E}\left[\left(\int_\Omega \xi\cdot G(\xi)\,\mathrm{d}x\right)^2\right]-\left(\mathbb{E}\left[\int_\Omega \xi\cdot G(\xi)\,\mathrm{d}x\right]\right)^2 =\\ &\qquad 2\sigma_1^4\left(\int_\Omega P_1\cdot G(P_1)\,\mathrm{d}x\right)^2+2\sigma_2^4\left(\int_\Omega P_2\cdot G(P_2)\,\mathrm{d}x\right)^2\\ &\qquad\quad+\sigma_1^2\sigma_2^2\left(\int_\Omega P_1\cdot G(P_2)\,\mathrm{d}x+\int_\Omega P_2\cdot G(P_1)\,\mathrm{d}x\right)^2. \quad (27)\end{aligned}$$

Finally, replacing the previous equation (27) in Eq. (26), calling $u=G(f)$ and $U_i=G(\sigma_i P_i)$ for $i=1,2$; we obtain the result.

□

Remark 5 *Using Equations* (17)-(22) *and* (24)-(25)*, Theorem 3 can be generalized to other cases. For instance, when* $m\geq 2$*,* ϵ_i *are not independent random variables or they do not follow a normal distribution.*

Remark 6 *We note that in the case of the random load* $f(\omega) = f + \varepsilon_1(\omega)P_1 + \varepsilon_2(\omega)P_2$ *and using Theorem 1, we get that any load* $F \in \mathrm{Conv}\{f, \sigma_1 P_1, \sigma_2 P_2, -f, -\sigma_1 P_1, -\sigma_2 P_2\}$ *satisfies that its compliance is bounded, more precisely*

$$\int_\Omega F \cdot U \,\mathrm{d}x \leq \max\left\{\int_\Omega f \cdot u \,\mathrm{d}x, \int_\Omega \sigma_1 P_1 \cdot U_1 \,\mathrm{d}x, \int_\Omega \sigma_2 P_2 \cdot U_2 \,\mathrm{d}x\right\}.$$

This can be generalized to $m \geq 2$ *perturbation functions.*

3.2 Considered minimization problem formulation

As mentioned previously, we are interested in solving minimization Problem (10). With the purpose of generating physically realizable optimized structures (see Section 1), we consider the so-called SIMP model (Solid Isotropic Material with Penalization; see [3, 2]). In this model, the set of admissible tensors is a subset M of the set $\hat{M}$, defined by (2), where the density $\eta(x) = \rho(x)^p,\ x \in \Omega$ with $p > 1$. In the previous formula, ρ corresponds to the design function of the considered optimization Problem (10). The reason of using ρ instead of η is that typical solutions have values of η either close to $\eta_{\min}$ or close to $\eta_{\max}$, with large gradients in between. The change of variable $\eta = \rho^p$ allows to deal with smother solution, easier to be found numerically (see [16]).

Considering the previous notations, minimization Problem (10) can be rewritten as

$$\begin{array}{rl} \min_\rho & \alpha\mathbb{E}[\Psi(\xi, K)] + \beta\,\mathrm{Var}[\Psi(\xi, K)] \\ \text{such that:} & \eta = \rho^p, \\ & K = \eta K^0, \\ & 0 \leq \int_\Omega \eta(x)\,\mathrm{d}x \leq V_{\max} \text{ and } \eta\colon \Omega \to [\eta_{\min}, \eta_{\max}], \end{array} \tag{28}$$

where, α and β are weight coefficients in [0,1]. The importance of their role and their impact on the solution is discussed in Section 5.1. Additionally, K^0 represents the fourth-order tensor of a linear elastic isotropic material, satisfying for all $u, v \in [H^1(\Omega)]^d$

$$e(v) : K^0 e(u) := 2\mu e(u)e(v) + \lambda \,\mathrm{div}\, u \,\mathrm{div}\, v, \tag{29}$$

where $AB = \sum_{i,j=1}^d a_{ij}b_{ij} = \mathrm{Tr}(AB^T)$; and μ, λ are the Lamé constants of the material (see e.g. [7, 1]).

However, the proposed definition of the set of admissible tensors in Problem (28) does not prevent that optimized solutions exhibit microstructures with periodic variation densities. As proposed in the literature (see, e.g. [2]), we tackle this problem indirectly by introducing a computational procedure in the numerical implementation of the minimization Problem (28) presented in the next section.

4 Numerical implementation of the model

In order to obtain a numerical approximated solution of Problem (28), for a finite representative set of values for (α, β) denoted by Σ, we consider the methodology described below.

To approximate the solution of System (1), we consider a finite element method (FEM), similar to the one proposed in [16]. Let N_x, N_y and N_z the number of elements in the X, Y and Z directions (the Z direction only applies in the 3D case), respectively, built by considering an equispaced discretization step size Δ_X, Δ_Y and Δ_Z, respectively. Thus, $N_{\text{el}} = N_x \times N_y$ and $N_{\text{el}} = N_x \times N_y \times N_z$ are the total number of elements used for the 2D and 3D cases, respectively. Furthermore, Θ denotes the set of all considered finite elements. We note that in [16], only the implementation of the 2D case is detailed. Thus, to help the reader to implement easily the 3D version, we give some details in A about the implementation of the 3D FEM model and the computation of the local stiffness matrix in $[0, 1]^3$.

Considering this FEM approach and a structure submitted to one main load and Np perturbation loads following a law $\mathcal{N}(0, 1)$ (such as the examples considered in Section 5), Problem (28) can be approximated by (see [2]-

Chapter 1.1.1)

$$\begin{aligned}\min_{\rho} J_{\text{opt}}(\rho) =& \alpha \left(\sum_{e\in\Theta} u_e^T K_e u_e + (\sum_{i=1}^{Np}(\sum_{e\in\Theta} U_{i,e}^T K_e U_{i,e})) \right) \\ &+ \beta \left((\sum_{i=1}^{Np}(\sum_{e\in\Theta} u_e^T K_e U_{i,e})^2) \right. \\ &\left. +(\sum_{i=1}^{Np}\sum_{j=1}^{Np}((\sum_{e\in\Theta} U_{j,e}^T K_e U_{i,e})(\sum_{e\in\Theta} U_{i,e}^T K_e U_{j,e}))) \right) \\ \text{such that } & :K_e = \rho_e^p K^0 \\ & 0 \le \sum_{e\in\Theta} \rho_e V_e \le V_{\max} \text{ and } \rho_e \in [\rho_{\min}, \rho_{\max}], \forall e.\end{aligned} \tag{30}$$

where $\rho = (\rho_e)_{e\in\Theta}$; ρ_e denotes the design function value at finite element $e \in \Theta$; V_e the volume or area of element e, according to the dimension 2 or 3 of the considered design problem, respectively; K_e denotes the element stiffness matrix at element e expressed in local coordinates (i.e., if $d = 2$ then $K_e \in \mathbb{R}^{8\times 8}$ and if $d = 3$ then $K_e \in \mathbb{R}^{24\times 24}$, see A); u_e is the vector of the deformations generated by the main load at the nodes of element e expressed in local coordinates (i.e., if $d = 2$ then $u_e \in \mathbb{R}^8$ and if $d = 3$ then $u_e \in \mathbb{R}^{24}$); $U_{i,e}$ is the vector of the deformations generated by the i-th perturbation load at the nodes of element e expressed in local coordinates.

Optimization Problem (30) is solved by using the Matlab package *Global Optimization Platform* (freely available at `http://www.mat.ucm.es/momat/software.htm`), where $N_{\text{OCM}} \in \mathbb{N}$ iterations of the optimal criteria method (OCM) described in [2] are used as the core algorithm and the initial condition is generated by using $N_{\text{sec}} \in \mathbb{N}$ iterations of a multi-layer secant method. The algorithm runs until the completion of all iterations. A complete description and validation of this methodology can be found in [10, 17, 15]. Here, we only give a brief description of the considered OCM. The evolution of the value of ρ_e from iteration i up to iteration $i + 1$ of the OCM is governed by:

$$\rho_e^{i+1} = \begin{cases} \max(\rho_{\min}, \rho_e^i - m) & \text{, if } \sqrt{B_e}\rho_e^i \le \max(\rho_{\min}, \rho_e^i - m), \\ \min(\rho_{\max}, \rho_e^i + m) & \text{, if } \sqrt{B_e}\rho_e^i \ge \min(\rho_{\max}, \rho_e^i + m), \\ \sqrt{B_e}\rho_e^i & \text{, else,} \end{cases} \tag{31}$$

where $m \in \mathbb{R}^+$ is a positive move-limit (i.e., a value that limits the evolution of ρ_e^{i+1} from ρ_e^i); $B_e = \left(- \widehat{\frac{\partial J_{\text{opt}}}{\partial \rho_e}}(\rho^i) \right) \Big/ \left(l \frac{\partial V(\rho^i)}{\partial \rho_e} \right)$; $\rho^i = (\rho_e^i)_{e \in \Theta}$; $V(\rho^i) = \sum_{e \in \Theta} \rho_e^i V_e$ is the material volume; l is a Lagrangian multiplier that can be found by a bi-sectioning algorithm; and $\widehat{\frac{\partial J_{\text{opt}}}{\partial \rho_e}}(\rho^i)$ is the mesh-independent filtered value of $\frac{\partial J_{\text{opt}}}{\partial \rho_e}(\rho^i)$, proposed in [18].

More precisely, as mentioned in Section 3.2, this filter is a numerical technique used to prevent the apparition of microstructures with periodic variation of densities in the numerical solutions (considering a FEM approach this phenomena is called check-board solutions, see [2]). To do so, $\widehat{\frac{\partial J_{\text{opt}}}{\partial \rho_e}}(\rho^i)$ is computed by considering a weighted average of $\frac{\partial J_{\text{opt}}}{\partial \rho_m}(\rho^i)$, for elements m which are in the ball $B(e, r_{\min})$ of radius $r_{\min}$ centered at the center of mass of element e, as following:

$$\widehat{\frac{\partial J_{\text{opt}}}{\partial \rho_e}}(\rho^i) = \sum_{m \subset B(e, r_{\min})} \frac{\rho_m (r_{\min} - \text{dist}(e, m))}{\rho_e \sum_{n \subset B(e, r_{\min})} (r_{\min} - \text{dist}(e, n))} \frac{\partial J_{\text{opt}}}{\partial \rho_m}(\rho^i), \tag{32}$$

where $\text{dist}(a, b)$ is the euclidean distance between the centers of mass of elements a and b; and $\frac{\partial J_{\text{opt}}}{\partial \rho_e}(\rho^i)$ is calculated as (see [2]-Chapter 1.2.3)

$$\begin{aligned} \frac{\partial J_{\text{opt}}}{\partial \rho_e}(\rho^i) =& p \rho_e^{p-1} \left(\alpha \left(-u_e^T K_e u_e - \sum_{i=1}^{Np} (U_{i,e}^T K_e U_{i,e}) \right) \right. \\ & - \beta \left((\sum_{i=1}^{Np} U_{i,e}^T K_e U_{i,e}) \, 2 (\sum_{i=1}^{Np} \sum_{j=i}^{Np} U_{j,e}^T K_e U_{i,e} (\sum_{m \in \Theta} U_{i,m}^T K_m U_{j,m})) \right. \\ & \left. \left. + \, 2 (\sum_{i=1}^{Np} u_e^T K_e U_{i,e} (\sum_{m \in \Theta} u_m^T K_m U_{i,m})) \right) \right). \end{aligned} \tag{33}$$

More details about the considered OCM can be found in [16, 2].

The solution of Problem (30), with fixed values of (α, β), given by our optimization approach is denoted by $\rho_{(\alpha,\beta)}$ and the associated density by $\eta_{(\alpha,\beta)} = \rho_{(\alpha,\beta)}^p$.

5 Numerical examples

In this Section, we present numerical experiments used to illustrate the interest the Variance-Expected compliance model proposed previously. To this aim, in Section **??**, we describe the considered 2D and 3D benchmark structures to be optimized by our approach and give the value of the model coefficients. Then, in Section 5.1, we show and analyse the results given by our methodology.

5.1 Considered benchmark problems

During this work, Problem (30) is solved by considering four particular benchmark structures, presented in both 2D and 3D versions. The interest of the 2D approach is to obtain a fine approximation of the solution whereas the 3D case allows to consider an additional perturbation direction and its impact on the structure. The benchmark structures studied here are some of the classical ones used to check the efficiency of structural optimization methods [2]. More precisely, we study:

a) Michel: This structure is a square horizontal cantilever and supports a vertical load.

Considering the 2D version, we study a domain $\Omega_{2D,M} = [0, 250] \times [0, 250]$. The side $\{0\} \times [0, 250]$ is assumed fixed. $V_{\max}$ is set to 25000. A point load $g = (0, -1)$ and a random load $(\varepsilon, 0)$, with $\varepsilon \sim \mathcal{N}(0, 1)$, are applied at node $(250, 0)$ (i.e. load g is identified by the node (250,0) and the vector (0,-1) so that $\int_{\Gamma_g} g.v\mathrm{d}x = (0, -1) \cdot v(250, 0), \forall v \in H$. We do not repeat this explanation in the following cases). This problem is denoted by **MICH2D**.

In the 3D problem, the structure is defined by the domain $\Omega_{3D,M} = [0, 20] \times [0, 20] \times [0, 20]$. The face $\{0\} \times [0, 20] \times [0, 20]$ is fixed and $V_{\max} = 2400$. A main point load $g = (0, 0, -1)$ is applied at the node $(20, 10, 0)$. At the same node, we consider a random point load $\xi = \varepsilon_1 P_1 + \varepsilon_2 P_2$, with ε_1 and ε_2 following $\mathcal{N}(0, 1)$, $P_1 = (1, 0, 0)$ and $P_2 = (0, 1, 0)$. This problem is denoted by **MICH3D**.

b) Dome: This structure is a vertical square that support a vertical load.

In the 2D case, we consider a domain $\Omega_{2D,D} = [0, 250] \times [0, 250]$ and the side $[0, 250] \times \{0\}$ is fixed. $V_{\max}$ is set to 25000. A point load

$g = (0, -1)$ and a random load $(\varepsilon, 0)$, with $\varepsilon \sim \mathcal{N}(0, 1)$, are applied at node $(125, 250)$. This problem is denoted by **DOME2D**.

The 3D structure is the domain $\Omega_{3D,D} = [0, 20] \times [0, 20] \times [0, 20]$. The face $[0, 20] \times [0, 20] \times \{0\}$ is fixed and $V_{\max} = 2400$. A point load $g = (0, 0, -1)$ is applied at the node $(10, 10, 20)$. Furthermore, at this node we consider a random point load $\xi = \varepsilon_1 P_1 + \varepsilon_2 P_2$, with ε_1 and ε_2 following $\mathcal{N}(0, 1)$, $P_1 = (1, 0, 0)$ and $P_2 = (0, 1, 0)$. This problem is denoted by **DOME3D**.

c) Cantilever: This problem consists in designing a non-square horizontal cantilever supporting a vertical load.

In its 2D version, we consider a domain $\Omega_{2D,C} = [0, 720] \times [0, 90]$. The side $\{0\} \times [0, 90]$ is fixed. The maximum amount of material is set to $V_{\max} = 25920$. A main point load $g = (0, -1)$ is applied at node $(720, 45)$. A random load $(\varepsilon, 0)$ with ε following a law $\mathcal{N}(0, 1)$ is applied to the same node. This problem is denoted by **CANT2D**.

In the 3D case, we consider a rectangular domain $\Omega_{3D,C} = [0, 80] \times [0, 10] \times [0, 10]$, The face $[0, 10] \times \{0\} \times [0, 10]$ of $\Omega_{3D,C}$ is fixed. The total amount of material is $V_{\max} = 2400$. A main point load $g = (0, 0, -1)$ is applied at the node $(80, 5, 5)$. We consider a random point load $\xi = \varepsilon_1 P_1 + \varepsilon_2 P_2$, with ε_1 and ε_2 random variables of law $\mathcal{N}(0, 1)$, $P_1 = (1, 0, 0)$ and $P_2 = (0, 1, 0)$, applied at the same node as g. This problem is denoted by **CANT3D**.

d) Bridge: This structure is an horizontal bridge supporting vertical loads on its upper face. For reducing the computational complexity of this problem all those loads are assumed to be equals.

In its 2D version, the domain is $\Omega_{2D,D} = [0, 360] \times [0, 180]$ and the sides $\{0\} \times [0, 180]$ and $\{360\} \times [0, 180]$ are fixed. $V_{\max}$ is set to 25920. Loads $g = (0, -1)$ and random loads $(\varepsilon, 0)$, with ε following a law $\mathcal{N}(0, 1)$, are applied to all points with coordinates $(x, 180)$, where $x \in \mathbb{N} \cap [0, 360]$. This problem is denoted by **BRID2D**.

In the 3D case, the domain $\Omega_{3D,D} = [0, 10] \times [0, 40] \times [0, 20]$. The faces $[0, 10] \times \{0\} \times [0, 20]$ and $[0, 10] \times \{40\} \times [0, 20]$ are fixed. $V_{\max}$ is set to 2400. Loads $g = (0, 0, -1)$ and random loads $\xi = \varepsilon_1 P_1 + \varepsilon_2 P_2$, with ε_1 and ε_2 following $\mathcal{N}(0, 1)$, $P_1 = (1, 0, 0)$ and $P_2 = (0, 1, 0)$ are applied to

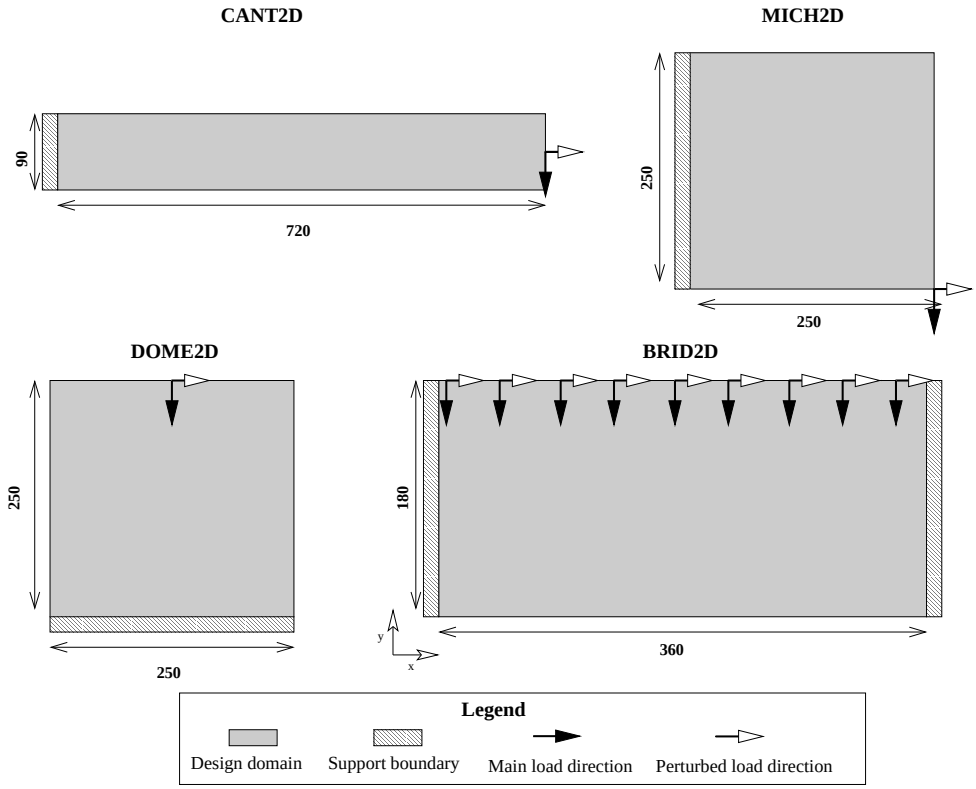

Figure 2: Geometrical representation of the 2D benchmark problems **CANT2D**, **MICH2D**, **DOME2D** and **BRID2D**.

nodes $(x, y, 20)$, where $x \in \mathbb{N} \cap [0, 10]$ and $y \in \mathbb{N} \cap [0, 40]$. This problem is denoted by **BRID3D**.

A geometrical representation of the 2D and 3D domains of the benchmark problems explained above is given in Figures 2 and 3, respectively. We note that problems **MICH3D** and **DOME3D** were studied in [10] in the case of optimizing truss structures submitted to random loads, which can be considered as a discrete version of the problems solved here.

The solution of those benchmark Problems are approximated by considering the numerical implementation described in Section 4 and the representative values $(\alpha, \beta) \in \Sigma := \{(1, 0), (0.75, 0.25), (0.5, 0.5), (0.25, 0.75), (0, 1)\}$ (see [10]). Furthermore, we set $\Delta_X = \Delta_Y = \Delta_Z = 1$, $\eta_{\min} = 10^{-3}$, $\eta_{\max} = 1$, $\lambda = 0.58$, $\mu = 0.38$, $r_{\min}$=1.5 and $p = 3$ (see [16]); $N_{\mathrm{OCM}} = 500$ and $N_{\mathrm{sec}} = 5$

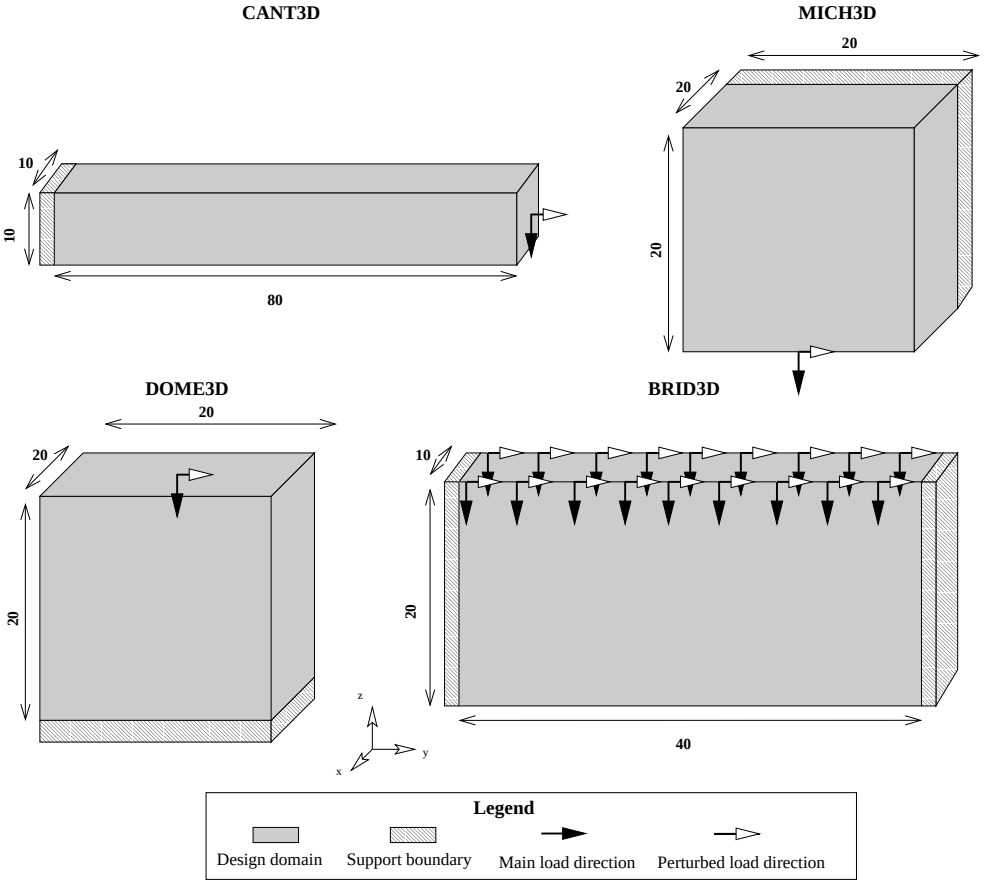

Figure 3: Geometrical representation of the 2D benchmark problems **CANT3D**, **MICH3D**, **DOME3D** and **BRID3D**.

(see [10]).

Moreover, we also solve numerically the problem of minimizing the compliance value of the structure submitted to the main load g without perturbation load. The density associated to the solution of this last problem is denoted by η_{comp}.

For each benchmark problem, in order to have a qualitative comparison of densities $\{\eta_{(\alpha,\beta)}\}_{(\alpha,\beta)\in\Sigma}$ and η_{comp}, we analyze their robustness when they are submitted to random loads and their density distribution. For this purpose, we first compute the compliance value, the expected compliance value and the variance value of each structure. Then, for each $\eta_{(\alpha,\beta)}$, we consider the random variable $\Phi_{\eta_{(\alpha,\beta)}} = \Psi(\xi, \eta_{(\alpha,\beta)})$. We approximate the density function of $\Phi_{\eta_{(\alpha,\beta)}}$, denoted by $\gamma_{\Phi_{\eta_{(\alpha,\beta)}}}$, by using a Monte-Carlo approach [15] that generates $M \in \mathbb{N}$ possible scenarios (i.e., values of ξ). Then, we calculate two representative statistical values of $\gamma_{\Phi_{\eta_{(\alpha,\beta)}}}$ associated to extreme scenarios (i.e., scenarios generating high compliance values in the structure): its maximum value and its ν%-Coherent-Value at Risk (C-VaR$_\nu$).

The ν%-Coherent-Value at Risk (C-VaR) is a risk measure defined as:

$$\text{C-VaR}_\nu(\chi) = \frac{1}{\nu}\int_0^\nu \inf\left\{z \in \mathbb{R} \text{ s.t. } \int_0^z 100\nu_\chi(x)\mathrm{d}x > (100-y)\right\}\mathrm{d}y,$$

where ν is a percentile, $\chi \in L^\infty(\mathcal{B}, \mathcal{F}, \mathbb{P})$, $(\mathcal{B}, \mathcal{F}, \mathbb{P})$ is a probability space, and ν_χ is the density function of χ. C-VaR$_\nu$ corresponds to the average value of the worst ν % case scenarios of χ (i.e., the ν % highest values of χ). A presentation and an application of C-VaR can be found in [15]. In our case, we have $\chi = \Phi_{\eta_{(\alpha,\beta)}}$.

As done in [10], we consider $M = 1000$ and $\nu = 5\%$.

5.2 Results

The results found during the numerical experiments presented in Section 4 are summarized in Tables 1 and 2 for the 2D and 3D benchmark problems, respectively. The 2D density distributions $\eta_{(\alpha,\beta)}$, when $(\alpha, \beta) \in \Sigma$ for the **MICH2D**, **DOME2D**, **CANT2D** and **BRID2D** cases are shown in Figures 4, 5, 6 and 7, respectively. The 3D density distribution $\eta_{(\alpha,\beta)}$, when $(\alpha, \beta) \in \Sigma$ for the **MICH3D**, **DOME3D**, **CANT3D** or **BRID3D** problems are depicted in Figures 8, 9, 10 and 11, respectively.

As the benchmark cases studied here are quite numerous and the conclusions are similar between them, we will only exhibit some general tendencies

	η_{comp}	$\eta_{(1,0)}$	$\eta_{(0.75,0.25)}$	$\eta_{(0.5,0.5)}$	$\eta_{(0.25,0.75)}$	$\eta_{(0,1)}$
MICH2D						
Comp	1,33	1,38	1,41	1,44	2,01	3,85
EC	2,41	2,22	2,23	2,25	2,74	4,61
Vari	38,5	23,7	22,0	21,9	22,0	48,0
C-VaR$_5$	6,32	5,44	5,37	4,71	5,89	9,42
Max	13,0	11,9	10,8	10,2	15,0	21,5
DOME2D						
Comp	0,25	0,30	0,31	0,32	0,33	0,47
EC	3,05	1,22	1,25	1,28	1,36	1,89
Vari	156	21,6	18,8	17,5	16,6	10,3
C-VaR$_5$	11,7	4,38	3.90	3,83	4,13	6,49
Max	36,1	12,0	8,70	8,62	11,9	17,7
CANT2D						
Comp	13,6	14,0	14,2	14,9	17,3	29,2
EC	14,9	13,8	14,2	14,5	17,5	29,3
Vari	52,2	14,8	3,83	3,73	3,36	3,31
C-VaR$_5$	16,1	15,4	14,6	14,5	17,8	29,6
Max	18,4	17,0	15,2	16,5	18,7	30,1
BRID2D						
Comp	1,09	1,21	1,22	1,23	1,25	1,66
EC	2,74	1,60	1,61	1,61	1,65	1,98
Vari	5412	382	336	321	279	206
C-VaR$_5$	7,10	2,76	2,70	2,56	2,48	2,91
Max	19,9	5,35	4,16	5,16	3,77	4,78

Table 1: Summary of the results obtained considering the densities η_{comp}, $\eta_{(1,0)}$, $\eta_{(0.75,0.25)}$, $\eta_{(0.5,0.5)}$, $\eta_{(0.25,0.75)}$ and $\eta_{(0,1)}$ for the Problems **MICH2D**, **DOME2D**, **CANT2D** and **BRID2D**: Compliance (**Comp**), Expected compliance (**EC**), Variance of the compliance (**Vari**), maximum compliance value (**Max**) and Coherent Value at Risk of the compliance (**C-VaR**$_5$).

	η_{comp}	$\eta_{(1,0)}$	$\eta_{(0.75,0.25)}$	$\eta_{(0.5,0.5)}$	$\eta_{(0.25,0.75)}$	$\eta_{(0,1)}$
MICH3D						
Comp	1,92	2,09	2,13	2,15	2,16	4,98
EC	6,76	5,32	5,57	5,59	5,61	8,51
Vari	27,9	14,1	14,0	14,0	12,3	10,5
C-VaR$_5$	16,9	13,1	12,5	12,7	12,5	16,7
Max	54,7	27,2	23,8	25,7	29,0	35,5
DOME3D						
Comp	0,68	0,71	0,74	0,76	0,79	0,80
EC	4,32	3,06	3,12	3,18	3,23	3,41
Vari	13,1	5,34	5,27	5,15	4,81	4,72
C-VaR$_5$	10,6	7,11	7,26	7,42	7,83	7,97
Max	32,9	19,4	18,5	19,5	19,8	21,1
CANT3D						
Comp	1,78	1,84	1,88	1,93	2,15	5,43
EC	6,62	3,67	3,70	3,72	4,08	6,88
Vari	4745	672	652	645	621	471
C-VaR$_5$	18,6	9,15	8,62	8,20	8,57	10,8
Max	51,4	24,2	22,1	21,3	21,6	25,3
BRID3D						
Comp	0,21	0,27	0,28	0,29	0,31	0,37
EC	1,89	0,73	0,73	0,75	0,76	0,84
Vari	4621	391	315	307	298	236
C-VaR$_5$	5,67	1,95	1,92	1,79	1,80	2,12
Max	15,5	5,62	4,89	5,12	5,56	6,09

Table 2: Summary of the results obtained considering the densities η_{comp}, $\eta_{(1,0)}$, $\eta_{(0.75,0.25)}$, $\eta_{(0.5,0.5)}$, $\eta_{(0.25,0.75)}$ and $\eta_{(0,1)}$ for the Problems **MICH3D**, **DOME3D**, **CANT3D** and **BRID3D**: Compliance (**Comp**), Expected compliance (**EC**), Variance of the compliance (**Vari**), maximum compliance value (**Max**) and Coherent Value at Risk of the compliance (**C-VaR**$_5$).

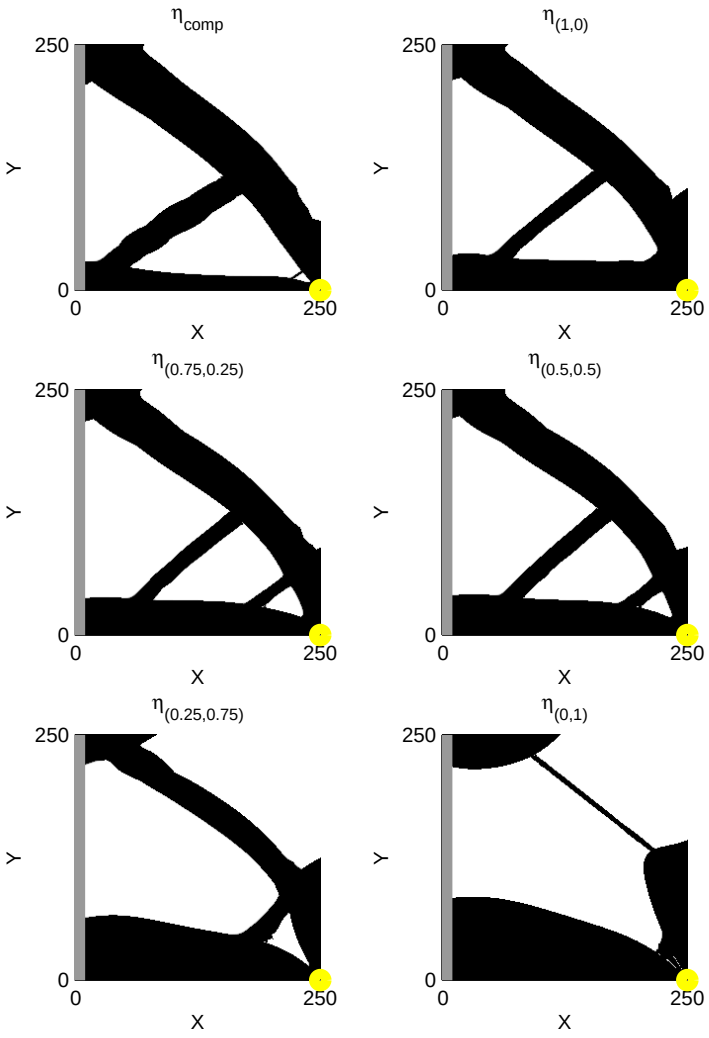

Figure 4: Density distribution η_{comp}, $\eta_{(1,0)}$, $\eta_{(0.75,0.25)}$, $\eta_{(0.5,0.5)}$, $\eta_{(0.25,0.75)}$ and $\eta_{(0,1)}$ obtained for the **MICH2D** Problem. The support is presented by a grey rectangle at position $x = 0$. The node where loads are applied are represented by a bright circle.

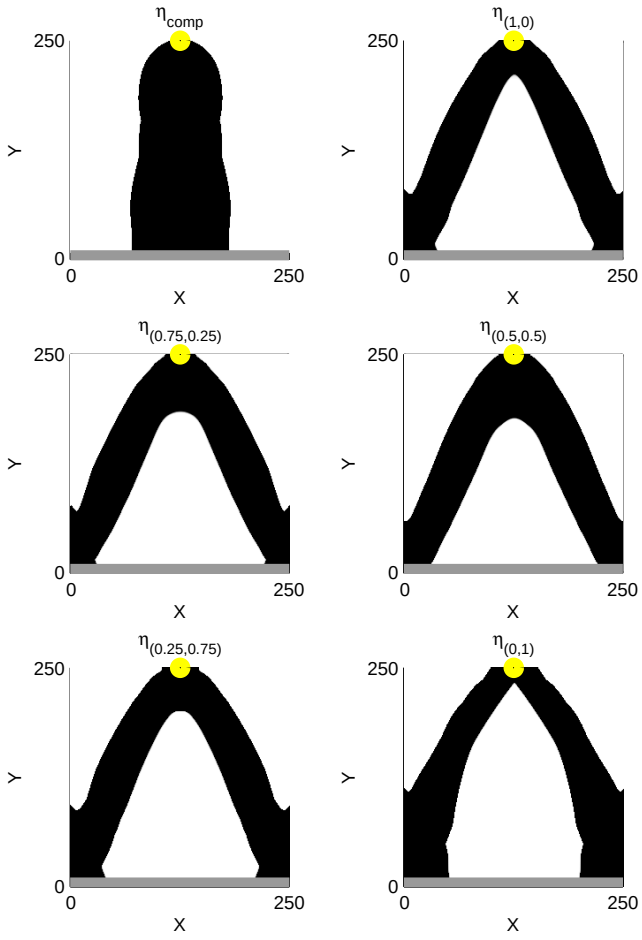

Figure 5: Density distribution η_{comp}, $\eta_{(1,0)}$, $\eta_{(0.75,0.25)}$, $\eta_{(0.5,0.5)}$, $\eta_{(0.25,0.75)}$ and $\eta_{(0,1)}$ obtained for the **DOME2D** Problem. A support wall is presented by a grey rectangle at position $y = 0$. The node where loads are applied are represented by a bright circle.

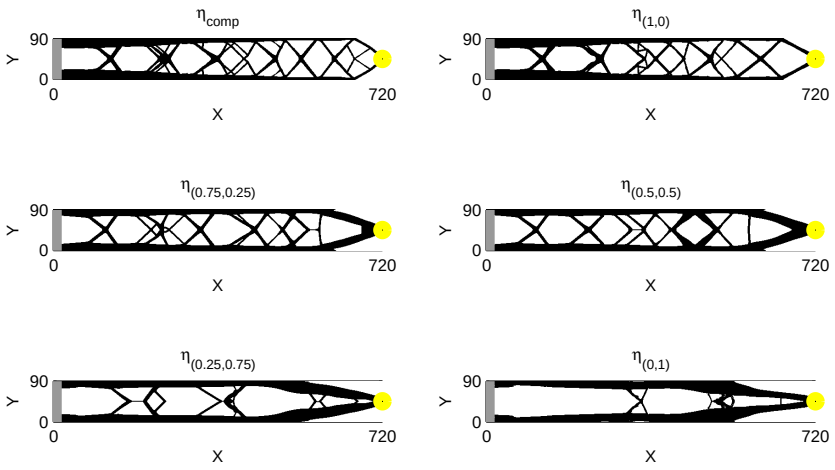

Figure 6: Density distribution η_{comp}, $\eta_{(1,0)}$, $\eta_{(0.75,0.25)}$, $\eta_{(0.5,0.5)}$, $\eta_{(0.25,0.75)}$ and $\eta_{(0,1)}$ obtained for the **CANT2D** Problem. The support is presented by a grey rectangle at position $x = 0$.

regarding the behaviour of our model when considering different values of α and β.

We can observe in Tables 1 and 2, that minimizing only the compliance and not considering the expected compliance nor the variance (i.e., η_{comp}), we obtain structures robust to the main load (i.e., for each problem, η_{comp} shows the lowest compliance value). However, η_{comp} is generally less stable to load perturbations than the structures from $\eta(1,0)$ up to $\eta_{(0.25,0.75)}$, as its Maximum and C-VaR$_5$ compliance values estimated during the Monte-Carlo approach are the highest ones. For instance, when considering the **DOME2D** case, the C-VaR$_5$ and Maximum compliance values of η_{comp} are 11,7 and 36.1, respectively, which represent an increase of 300% when regarding the C-VaR$_5$ and Maximum compliance values of $\eta_{(1,0)}$ up to $\eta_{(0.25,0.75)}$. In counterpart, the compliance values of $\eta_{(1,0)}$ up to $\eta_{(0.25,0.75)}$ are only between 20% and 30% higher than the η_{comp} one. This seems to indicate that considering the Variance-Expected Compliance model should help to generate structures better adapted to perturbed loads scenarios (i.e., which present reduced deformations in cases of severe perturbations) than the classical com-

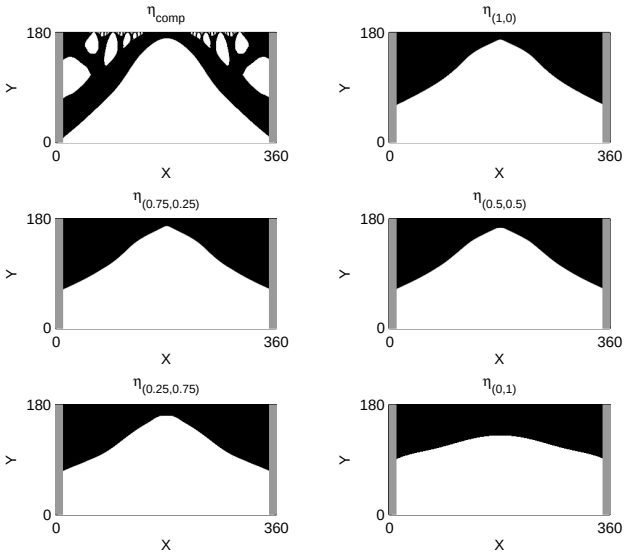

Figure 7: Density distribution η_{comp}, $\eta_{(1,0)}$, $\eta_{(0.75,0.25)}$, $\eta_{(0.5,0.5)}$, $\eta_{(0.25,0.75)}$ and $\eta_{(0,1)}$ obtained for the **BRID2D** Problem. The supports are presented by a grey rectangles at position $x = 0$ and $x = 360$. For a better understanding of the densities, the loads are not shown.

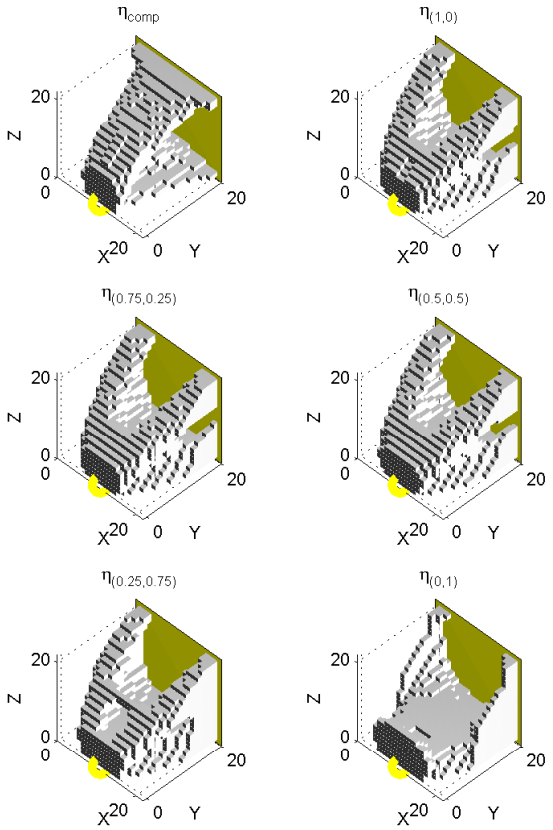

Figure 8: Density distribution η_{comp}, $\eta_{(1,0)}$, $\eta_{(0.75,0.25)}$, $\eta_{(0.5,0.5)}$, $\eta_{(0.25,0.75)}$ and $\eta_{(0,1)}$ obtained for the **MICH3D** Problem. One support is presented by a filled plane at position $x = 0$. The node where loads are applied are represented by a bright circle.

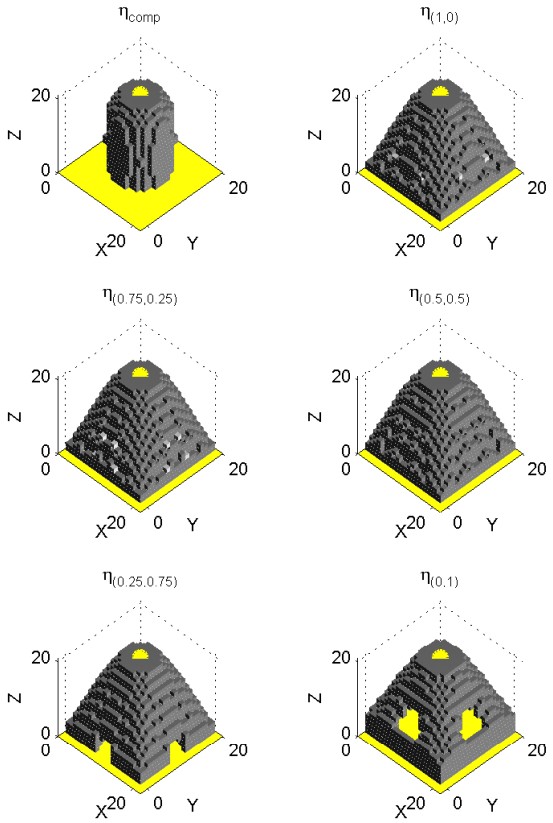

Figure 9: Density distribution η_{comp}, $\eta_{(1,0)}$, $\eta_{(0.75,0.25)}$, $\eta_{(0.5,0.5)}$, $\eta_{(0.25,0.75)}$ and $\eta_{(0,1)}$ obtained for the **DOME3D** Problem. One of the support walls is presented by a filled plane at position $x = 0$. The node where loads are applied are represented by a bright circle.

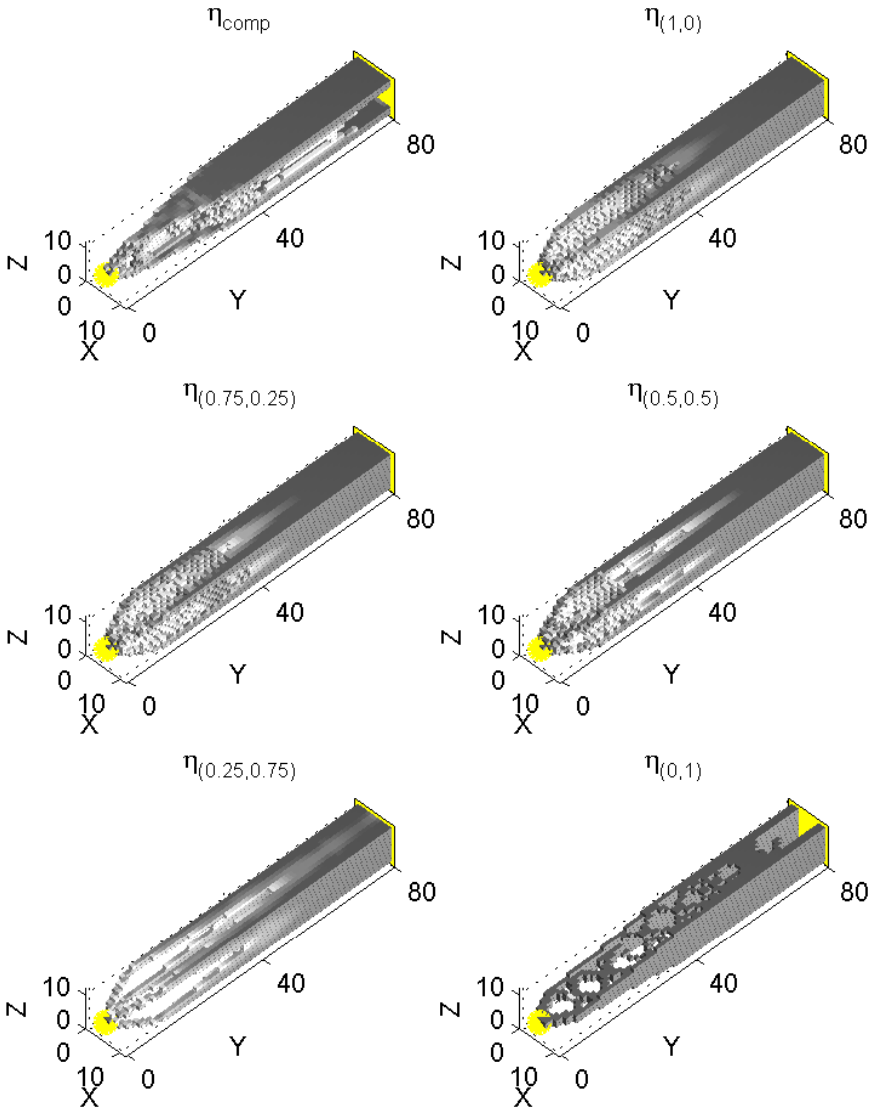

Figure 10: Density distribution η_{comp}, $\eta_{(1,0)}$, $\eta_{(0.75,0.25)}$, $\eta_{(0.5,0.5)}$, $\eta_{(0.25,0.75)}$ and $\eta_{(0,1)}$ obtained for the **CANT3D** Problem. The support is presented by a filled plane at position $x = 0$. The node where loads are applied are represented by a bright circle.

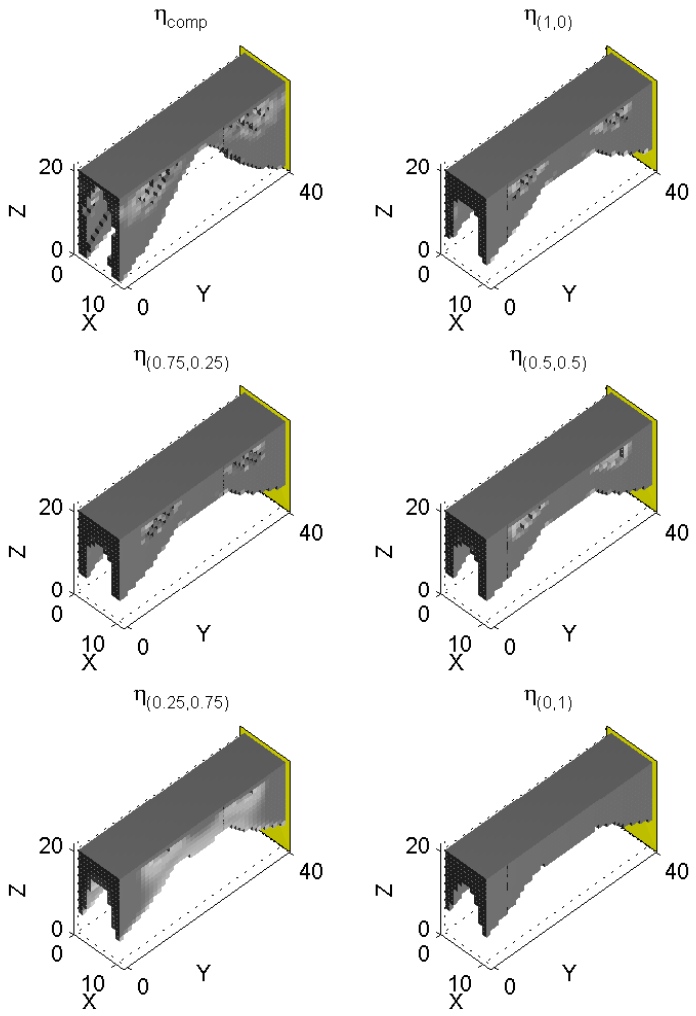

Figure 11: Density distribution η_{comp}, $\eta_{(1,0)}$, $\eta_{(0.75,0.25)}$, $\eta_{(0.5,0.5)}$, $\eta_{(0.25,0.75)}$ and $\eta_{(0,1)}$ obtained for the **BRID3D** Problem. A support wall is presented by a filled plane at position $x = 0$. For a better understanding of the densities, the other support wall and loads are not shown.

pliance model. However, the choice of (α, β) is important as in some rare cases, the $\eta_{(\alpha,\beta)}$ structure exhibits worst characteristics than η_{comp}. For example, in the **CANT2D** Problem, $\eta_{(0.25,0.75)}$ and $\eta_{(0,1)}$ have higher compliance, C-VaR$_5$ and Maximum compliance values than η_{comp}.

When comparing the effect of the weight coefficients (α, β) on the solutions, we can observe that if our objective is to reduce the extreme scenarios compliance (i.e., reduce the C-VaR$_5$ or the Maximum compliance values) both values α and β should be strictly positive. For instance, for the **CANT3D** Problem, $\eta_{(0.25,0.75)}$ shows the lowest C-VaR$_5$ and maximum compliance values whereas, for the **BRID3D** case, $\eta_{(0.5,0.5)}$ is the most resilient structure to strong perturbations. This seems to indicate that for each particular design problem, if we are interested in managing severe perturbations, a previous study on the values of (α, β) should be performed in order to determine their optimal values. This interpretation can be also observed on Figure 12, where a boxplot representation[2] of the density functions of the random variable associated to the compliance value of η_{comp}, $\eta_{(1,0)}$, $\eta_{(0.75,0.25)}$, $\eta_{(0.5,0.5)}$, $\eta_{(0.25,0.75)}$ and $\eta_{(0,1)}$ obtained during Problem **CANT2D** is presented. We can see that the boxplots becomes thinner as β increases (i.e., the variance decreases) and their maximum values decreases up to a certain value of β (here, .25) from which the maximum compliance value start to growth.

From a general point of view, when we raise β the value of the variance of the compliance decreases and the expected compliance increases. Indeed, as observed in the truss case [10], when we increase the variance weight, we increase the robustness of the structure to the perturbed loads whereas it becomes weaker to the main load. This can be observed on the evolution of the density distribution $\eta_{(\alpha,\beta)}$ in function of (α, β). More precisely, regarding Figures 4 and 8, for the **MICH2D** and **MICH3D** cases, there is a mass transfer phenomena when β increases from the diagonal 'bars' (supporting the vertical main load) to the floor of the structure (which offer a good resistance to the perturbed loads in the plane $z = 0$). Considering the **DOME2D** and **DOME3D** cases, there is a material transfer when β raises from the upper part of the dome (sustaining the main load) to the 'feet' of the structure (which offer resistance to horizontal perturbations). The same mass transfer phenomena were also observed for the Michel and Dome cases

[2]Boxplots are composed by a box, which has lines at the lower quartile, median, and upper quartile values, and whiskers that extend from each end of the box to the lower and higher compliance value [19].

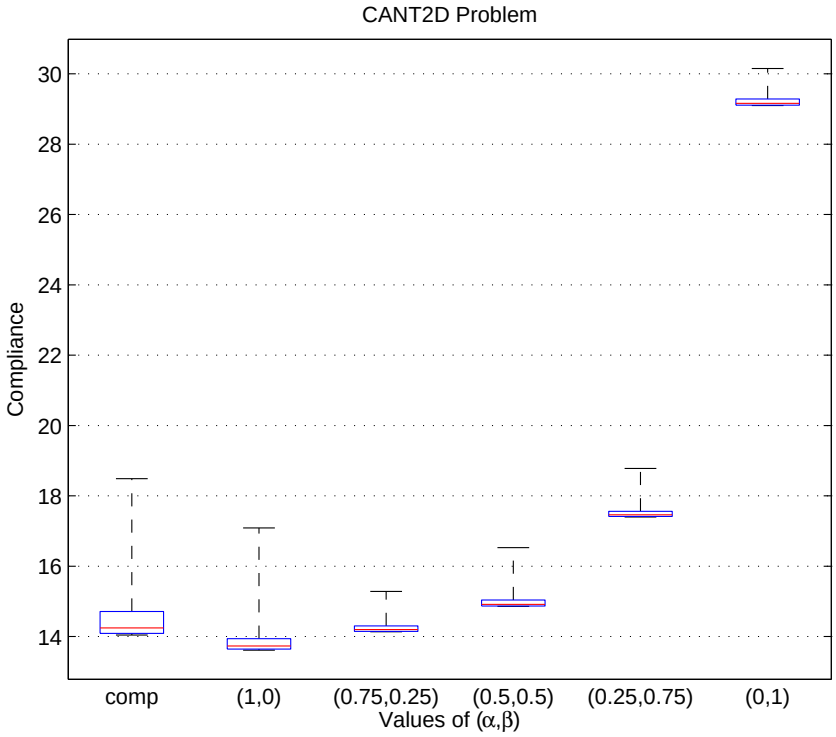

Figure 12: Boxplot representation of the compliance value density functions of η_{comp}, $\eta_{(1,0)}$, $\eta_{(0.75,0.25)}$, $\eta_{(0.5,0.5)}$, $\eta_{(0.25,0.75)}$ and $\eta_{(0,1)}$ obtained for the **CANT2D** Problem.

considering truss structures in Ref. [10]. For the **CANT2D** and **CANT3D** structures, we can see on Figures 6 and 10 that when α decreases, the matter that compound the net of internal bars (offering resistance to vertical loads) is progressively redistributed to the lateral parts of the structure (adapted to horizontal loads). Finally, for the **BRDI2D** and **BRID3D** structures, we observe on Figures 7 and 11, that the mass transfer occurs from the columns linking the bridge with the lateral supports to the upper part of the bridge (well suited to sustain the horizontal perturbations). A graphical representation of this phenomenon can be observed on Figures 13 and 14 which depict the deformation of structure $\eta_{(1,0)}$ and $\eta_{(0,1)}$ in the **CANT3D** case when they are submitted to vertical and horizontal loads. We can observe that $\eta_{(1,0)}$ is the most resistant to vertical deformation whereas $\eta_{(0,1)}$ is the most resistant to horizontal loads.

The rates of increase/decrease of the expected compliance and variance values according to the weight coefficients (α, β) depend on the studied design problem. For instance, on the one hand, during the **DOME3D** experiment, the expected compliance raises 12% and the variance decreases 12% when comparing $\eta_{(1,0)}$ with $\eta_{(0,1)}$. On the other hand, for the **BRID3D** case, the expected compliance is increased by 15% and the variance decreased by 40% when considering $\eta_{(1,0)}$ in front of $\eta_{(0,1)}$. As said previously, the choice of (α, β) should be adapted to the considered design problem.

6 Conclusions

During this work, we have presented a Variance-Expected Compliance model, originally proposed for truss structures, to solve stochastic topology optimization problems. The behaviour of this model was studied numerically by considering a finite element implementation and various 2D and 3D benchmark cases. The obtained results seem to indicate that considering our formulation with adequate weight coefficients allow to generate structure robust to main loads and their perturbations in case of extreme scenarios. In future works, we aim to improve the algorithm proposed here, considering fast and efficient optimization methods. Additionally, we will consider probabilistic constraints in the framework of reliability based optimization design.

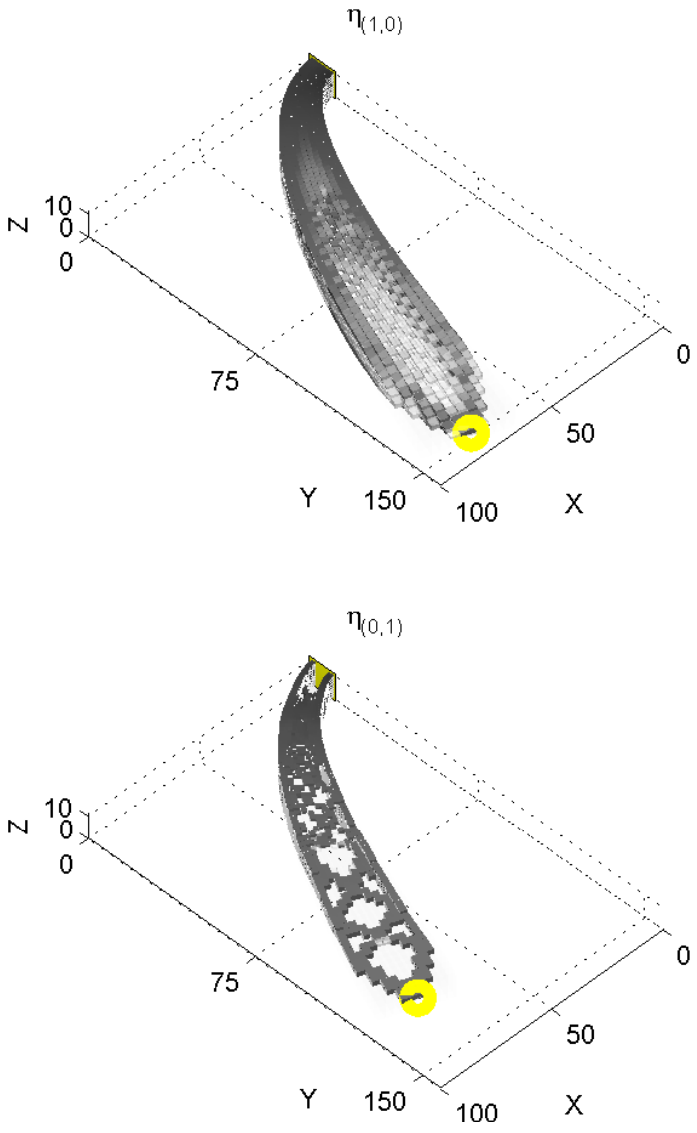

Figure 13: Deformation of the structures (**Up**) $\eta_{(1,0)}$ and (**Down**) $\eta_{(0,1)}$ obtained for the **CANT3D** Problem when submitted to the horizontal load (0,1,0) on point (80,5,5) (represented by a bright circle).

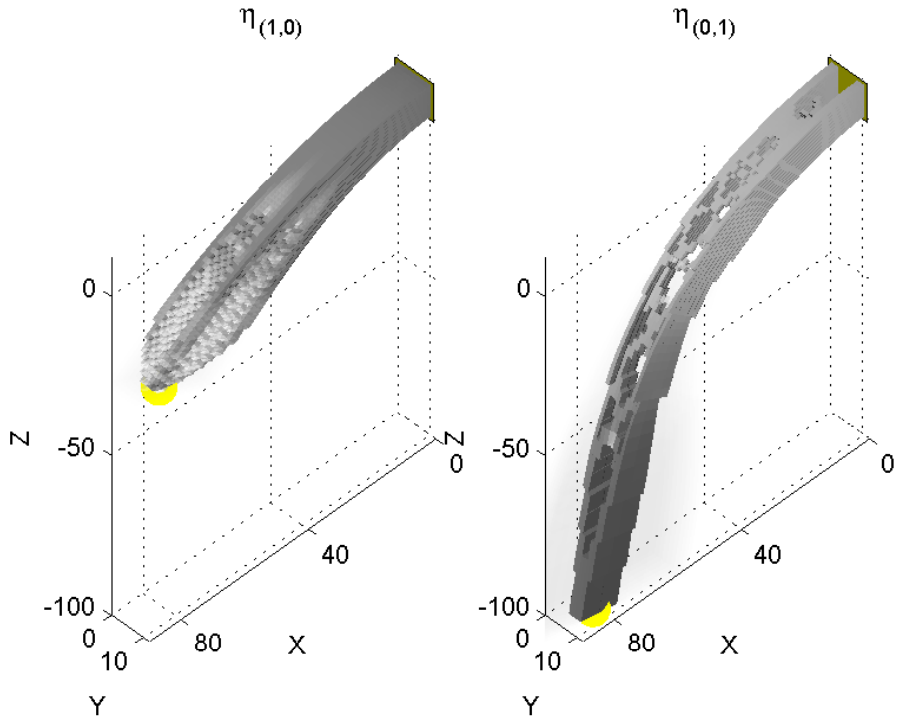

Figure 14: Deformation of the structures (**Up**) $\eta_{(1,0)}$ and (**Down**) $\eta_{(0,1)}$ obtained for the **CANT3D** Problem when submitted to the vertical load (0,0,-1) on point (80,5,5) (represented by a bright circle).

Acknowledgments

This work was carried out thanks to the financial support of the "Universidad de los Andes"; the Spanish " Ministry of Economy and Competitiveness" under project MTM2011-22658; the "Comunidad de Madrid" under project S2009/PPQ-1551; the "Junta de Andalucía" through project P12-TIC301; and the "FONDECYT" under grant 1130905.

A Computation of Stiffness Matrix

For the numerical analysis above we need to compute the *local stiffness matrix* of the element $T^* := [0,1]^d$ where d is set to 2 or 3. Whereas this computation is rather standard, we present here the main clues to construct the stiffness matrix of a single element in order to help the reader to repeat the results presented here for the finite element discretization. Also, we present a simple program written in Matlab to compute this matrix in the three dimensional case. Most of this part is based on the work of Alberti et al. [5] and Ciarlet [7, 6].

In the following we consider the finite dimensional space V_h, with $N = \dim(V_h)$, corresponding to a standard Galerkin representation of (1). We find $u_h \in V_h$ such that (4) is satisfied for all $v_h \in V_h$, i.e. we find

$$A(u_h, v_h) = \int_\Omega f \cdot v_h \, \mathrm{d}x \qquad \forall v_h \in V_h. \tag{34}$$

For $\{\psi_j\}_{1,\dots,N}$ a basis of V_h we get that solving (34) above is equivalent to find $U \in \mathbb{R}^N$ that solves the linear system $\{A\}U = \{b\}$, with

$$\{A\}_{ij} = A(\psi_i, \psi_j), \quad \text{and} \quad \{b\}_j = \int_\Omega f \cdot \psi_j \, \mathrm{d}x,$$

here $\{A\}$ is called the *global stiffness matrix* of the discretized problem (34). We assume that $\Omega = \cup_k T_k$, a partition on regular finite elements (see Ciarlet [7] for details). We get

$$\{A\}_{ij} = \sum_k \int_{T_k} e(\psi_i) : Ke(\psi_j) dx,$$

each element T_k corresponds to an affine transformation of the reference element T^*, thus in order to compute $\{A\}$ first we have to compute the local

stiffness matrix

$$\int_{T^*} e(\tilde{\psi}_i) : Ke(\tilde{\psi}_j)dx,$$

where $\{\tilde{\psi}_i\}$ corresponds to a basis of functions for the reference element T^*.

In the following section we compute the local stiffness matrix of the cubic element $T^* = [0,1]^3$, with K the fourth-order tensor of a linear elastic isotropic material, satisfying Eq. (29). Several examples of topology optimization, including the Matlab code for square elements can be found in Sigmund [16]. A short open-box Matlab implementation for computing the stiffness matrix for triangular, square, and tetrahedral family of finite elements can be found in Alberty et al. [5].

A.1 Cubic Elements

Let us consider the element $T^* = [0,1]^3$, we have the following scalar hat functions defined on T^*, with $x = (x_1, x_2, x_3)$:

$$\begin{array}{ll}
\varphi_1(x) = (1-x_1)(1-x_2)(1-x_3) & \varphi_2(x) = x_1(1-x_2)(1-x_3) \\
\varphi_3(x) = x_1x_2(1-x_3) & \varphi_4(x) = (1-x_1)x_2(1-x_3) \\
\varphi_5(x) = (1-x_1)(1-x_2)x_3 & \varphi_6(x) = x_1(1-x_2)x_3 \\
\varphi_7(x) = x_1x_2x_3 & \varphi_8(x) = (1-x_1)x_2x_3
\end{array}$$

Therefore, a basis of V_h (the finite dimension space approximating $L^2(\Omega)^d$) for the element T^* is given by

$$\{\tilde{\psi}_1, \ldots, \tilde{\psi}_{24}\} := \left\{ \begin{pmatrix} \varphi_1 \\ 0 \\ 0 \end{pmatrix}, \begin{pmatrix} 0 \\ \varphi_1 \\ 0 \end{pmatrix}, \begin{pmatrix} 0 \\ 0 \\ \varphi_1 \end{pmatrix}, \ldots, \begin{pmatrix} \varphi_8 \\ 0 \\ 0 \end{pmatrix}, \begin{pmatrix} 0 \\ \varphi_8 \\ 0 \end{pmatrix}, \begin{pmatrix} 0 \\ 0 \\ \varphi_8 \end{pmatrix} \right\}.$$

Using Voigt representation of the linear strain tensor we obtain that, for every $u, v \in [H^1(\Omega)]^d$, $e(u) : Ke(v) = \gamma(v)^t\{K\}\gamma(u)$, where

$$\{K\} = \begin{pmatrix} \lambda+2\mu & \lambda & \lambda & 0 & 0 & 0 \\ \lambda & \lambda+2\mu & \lambda & 0 & 0 & 0 \\ \lambda & \lambda & \lambda+2\mu & 0 & 0 & 0 \\ 0 & 0 & 0 & \mu & 0 & 0 \\ 0 & 0 & 0 & 0 & \mu & 0 \\ 0 & 0 & 0 & 0 & 0 & \mu \end{pmatrix} \quad \text{and} \quad \gamma(u) = \begin{pmatrix} \frac{\partial u_1}{\partial x_1} \\ \frac{\partial u_2}{\partial x_2} \\ \frac{\partial u_3}{\partial x_3} \\ \frac{\partial u_1}{\partial x_2} + \frac{\partial u_2}{\partial x_1} \\ \frac{\partial u_1}{\partial x_3} + \frac{\partial u_3}{\partial x_1} \\ \frac{\partial u_2}{\partial x_3} + \frac{\partial u_3}{\partial x_2} \end{pmatrix}. \tag{35}$$

Thus, the corresponding local stiffness matrix in the tree dimensional case is given by

$$\int_{T^*} \gamma(\tilde{\psi}_i)^t \{K\} \gamma(\tilde{\psi}_j) \mathrm{d}x \quad \text{for } i,j = 1,\ldots,24.$$

In order to compute the local stiffness matrix we have to compute the following quantities

$$[R_{kl}]_{ij} = \iiint_{T^*} \frac{\partial \varphi_i}{\partial x_k} \frac{\partial \varphi_j}{\partial x_l} \mathrm{d}x,$$

for $i,j = 1,\ldots,8$ and $k,l = 1,2,3$. It is not difficult to see that R_{11}, R_{22} and R_{33} are symmetric matrices, $R_{21} = R_{12}^t$ and also $R_{32} = R_{23}^t$.

Remark 7 *Similar computations can be made in the two dimensional case in order to obtain the stiffness matrix of the square element* $T^* = [0,1]^2$. *We can obtain the corresponding matrix* $\{K\}$ *by eliminating the coordinates associated to* u_3 *in* (35), *getting the so-called* Plane Strain *formulation. A more popular formulation for computing the stiffness matrix in the two dimensional case corresponds to that called* Plane Stress *formulation, where* $\{K\}$ *is given by:*

$$\{K\} = \begin{pmatrix} \lambda+2\mu & \lambda & 0 \\ \lambda & \lambda+2\mu & 0 \\ 0 & 0 & \mu \end{pmatrix} - \frac{\lambda^2}{\lambda+2\mu} \begin{pmatrix} 1 & 1 & 0 \\ 1 & 1 & 0 \\ 0 & 0 & 0 \end{pmatrix}. \tag{36}$$

The Plane Strain or Plane Stress formulations must be chosen according to the conditions of the problem.

We present below the Matlab code to compute the local stiffness matrix of the cubical element $[0,1]^3$ following the approach explained above.

```
lambda=0.576; mu=0.384;
R_11 = [4,-4,-2, 2, 2,-2,-1,1; -4,4,2,-2,-2,2,1,-1; -2,2,4,-4,
-1,1,2,-2; 2,-2,-4,4,1,-1,-2,2; 2,-2,-1,1,4,-4,-2,2; -2,2,1,-1,
-4,4,2,-2; -1,1,2,-2,-2,2,4,-4;1,-1,-2,2,2,-2,-4,4]/36;
R_22 = [4,2,-2,-4,2,1,-1,-2;2,4,-4,-2,1,2,-2,-1;-2,-4,4,2,-1,
-2,2,1; -4,-2,2,4,-2,-1,1,2; 2,1,-1,-2,4,2,-2,-4;1,2,-2,-1,2,
4,-4,-2; -1,-2,2,1,-2,-4,4,2;-2,-1,1,2,-4,-2,2,4]/36;
R_33 = [4,2,1,2,-4,-2,-1,-2;2,4,2,1,-2,-4,-2,-1;1,2,4,2,
-1,-2,-4,-2; 2,1,2,4,-2,-1,-2,-4;-4,-2,-1,-2,4,2,1,2;-2,-4,-2,
-1,2,4,2,1; -1,-2,-4,-2,1,2,4,2;-2,-1,-2,-4,2,1,2,4]/36;
```

```
R_12 = [2,2,-2,-2,1,1,-1,-1;-2,-2,2,2,-1,-1,1,1;-2,-2,2,2,-1,
-1,1,1; 2,2,-2,-2,1,1,-1,-1; 1,1,-1,-1,2,2,-2,-2;-1,-1,1,1,-2,
-2,2,2; -1,-1,1,1,-2,-2,2,2;1,1,-1,-1,2,2,-2,-2]/24;
R_13 = [2,2,1,1,-2,-2,-1,-1;-2,-2,-1,-1,2,2,1,1;-1,-1,-2,-2,1,
1,2,2; 1,1,2,2,-1,-1,-2,-2; 2,2,1,1,-2,-2,-1,-1;-2,-2,-1,-1,2,
2,1,1; -1,-1,-2,-2,1,1,2,2;1,1,2,2,-1,-1,-2,-2]/24;
R_23 = [2,1,1,2,-2,-1,-1,-2;1,2,2,1,-1,-2,-2,-1;-1,-2,-2,-1,1,
2,2,1; -2,-1,-1,-2,2,1,1,2;2,1,1,2,-2,-1,-1,-2;1,2,2,1,-1,
-2,-2,-1; -1,-2,-2,-1,1,2,2,1;-2,-1,-1,-2,2,1,1,2]/24;
L = [lambda+2*mu,lambda,mu];
KE = zeros(24,24);
KE([1:3:24],[1:3:24]) = L(1)*R_11 + L(3)*R_22+ L(3)*R_33;
KE([2:3:24],[2:3:24]) = L(3)*R_11 + L(1)*R_22+ L(3)*R_33;
KE([3:3:24],[3:3:24]) = L(3)*R_11 + L(1)*R_22+ L(3)*R_33;
KE([2:3:24],[1:3:24]) = L(3)*R_12 + L(2)*R_12';
KE([3:3:24],[1:3:24]) = L(3)*R_13 + L(2)*R_13';
KE([3:3:24],[2:3:24]) = L(3)*R_23 + L(2)*R_23';
KE([1:3:24],[2:3:24]) = KE([2:3:24],[1:3:24])';
KE([1:3:24],[3:3:24]) = KE([3:3:24],[1:3:24])';
KE([2:3:24],[3:3:24]) = KE([3:3:24],[2:3:24])';
```

Bibliography

References

[1] L. Landau, E. M. Lifshitz, Theory of Elasticity, Oxford, England: Butterworth Heinemann, 1986.

[2] M. Bendsøe, O. Sigmund, Topology Optimization: Theory, Methods and Applications, Springer-Verlag, Berlin, 2003.

[3] M. Bendsøe, Optimization of structural topology, shape, and material, Springer, 1995.

[4] S. Conti, H. Held, M. Pach, M. Rumpf, R. Schultz, Shape optimization under uncertainty, a stochastic programming perspective, SIAM Journal on Optimization 19 (4) (2008) 1610–1632.

[5] J. Alberty, C. Carstensen, S. A. Funken, , R. Klose, Matlab implementation of the finite element method in elasticity, Computing 3 (69) (2002) 269–263.

[6] P. Ciarlet, The Finite Element Method For Elliptic Problems, North-Holland, Amsterdam, 1980.

[7] P. Ciarlet, Mathematical Elasticity, Vol. I, Three Dimensional Elasticity., North-Holland, Amsterdam, Amsterdam, 1988.

[8] F. Alvarez, M. Carrasco, Minimization of the expected compliance as an alternative approach to multiload truss optimization, Struct. Multidiscip. Optim. 29 (6) (2005) 470–476.

[9] M. Carrasco, Diseño óptimo de estructuras reticulares en elasticidad lineal vía teoría de la dualidad. estudio teórico y numérico, Ph.D. thesis, Universidad de Chile, engineering Degree Thesis (2003).

[10] M. Carrasco, B. Ivorra, A. M. Ramos, A variance-expected compliance model for structural optimization, J. Optim. Theory Appl. 152 (1) (2012) 136–151.

[11] M. Carrasco, B. Ivorra, R. Lecaros, A. M. Ramos, An expected compliance model for topology optimization, Differ. Equ. Appl 4 (1) (2012) 111–120.

[12] J. Zhao, C. Wang, Robust topology optimization of structures under loading uncertainty, American Institute of Aeronautics and Astronautics Journal 2 (52) (2014) 398–407.

[13] G. Allaire, C. Dapogny, A linearized approach to worst-case design in parametric and geometric shape optimization, Mathematical Models and Methods in Applied Sciences in press (2014) 1–58.

[14] A. Ben-Tal, A. Nemirovski, Robust truss topology design via semidefinite programming, SIAM J. Optim. 7 (4) (1997) 991–1016.

[15] B. Ivorra, B. Mohammadi, A. M. Ramos, Optimization strategies in credit portfolio management, Journal Of Global Optimization. 2 (43) (2009) 415–427.

[16] O. Sigmund, A 99 line topology optimization code written in matlab, Structural and Multidisciplinary Optimization 2 (21) (2001) 120–127.

[17] B. Ivorra, D. Hertzog, B. Mohammadi, J. Santiago, Semi-deterministic and genetic algorithms for global optimization of microfluidic protein-folding devices, International Journal for Numerical Methods in Engineering 66 (2) (2006) 319–333.

[18] O. Sigmund, On the design of compliant mechanisms using topology optimization, Mechanics of Structures and Machines 25 (4) (1997) 493–524.

[19] J. Tukey, Exploratory Data Analysis, Addison-Wesley series in behavioral sciences, Addison-Wesley Publishing Company, 1977.